Using Terrestrial LiDAR to Monitor Erosion within the Gold Basin Landslide Complex, Verlot, WA

Coire McCabe

A report prepared in partial fulfillment of
the requirements for the degree of

Master of Science
Earth and Space Sciences: Applied Geosciences

University of Washington

March, 2016

Internship coordinator:
Kathy Troost

Reading committee:
Alison Duvall
Amit Mushkin

MESSAGe Technical Report Number: 028

Abstract

In 2014 the United States Forest Service closed the Gold Basin Campground of western Washington in an effort to protect the public from unstable hillslopes directly adjacent to the campground. The Gold Basin Landslide Complex (GBLC) is actively eroding via block fall, dry ravel, and debris flows, which contribute sediment into the South Fork of the Stillaguamish River. This sediment diminishes the salmonid population within the South Fork of the Stillaguamish River by reducing habitable spawning grounds, which is a big concern to the Stillaguamish Tribe of Indians. In this investigation, I quantified patterns of degradation and total volume of sediment erosion from the middle lobe of the GBLC over the period of July 2015 through January 2016 using terrestrial (ground-based) LiDAR (TLS). I characterized site specific stratigraphy and geomorphic processes, and laid the groundwork for future, long-term monitoring of this site.

Results of this investigation determined that ~ 4,800m^3 of sediment was eroded from the middle lobe of the GBLC during the 6 month study period (July 2015 – January 2016). This erosion likely occurred from debris flows, raveling of poorly sorted sand and gravel deposits and block failures of high plasticity silts and clays, and/or other mass wasting mechanisms. The generalized stratigraphic sequence in the GBLC consists of alternating massive beds of sand and gravel with silts and clays. The low permeability of these silts and clays provide a perfect venue for groundwater to percolate, as I observed during field investigations, which likely contributes to the active instability of the hillslopes. Continued monitoring and mapping of this complex will lead to viable information that could help both the United States Forest Service and the Stillaguamish Tribe of Indians.

Table of Contents

Table of Figures

Tables

Acknowledgements

I would like to acknowledge and thank the following groups for making this project possible. A big thank you goes to the United States Forest Service for granting access to Gold Basin Campground which has been closed to the public for the past two years. To the Stillaguamish Tribe of Indians for providing previous study documents regarding the Gold Basin Landslide Complex. To Professors Alison Duvall and Amit Mushkin for reviewing the written work and providing technical assistance regarding the terrestrial LiDAR post-processing. Professor Kathy Goetz Troost for providing significant support on the subject and organizing transportation to the field. My colleagues Pamela Wichgers, James Bush, and Amelia Oates for their support with field work in the treacherous terrain of the North Cascades. Finally, to Devin Bedard for his countless hours of help working on post-processing data, reviewing methodologies, field work, and late nights. This project would not have been possible without the help of these people.

1.0 Introduction

In May 2014, the United States Forest Service (USFS) closed the Gold Basin Campground, which is the biggest campground in the Mt. Baker-Snoqualmie National Forest, western Washington (Figure 1 and 2). This closure was due to an overwhelming threat of catastrophic failure of a hillslope directly north of the campground. This specific hillslope has been referred to as the Gold Basin Landslide (GBL) (Drury, 2001), but for the purposes of this investigation it is referred to as the Gold Basin Landslide Complex (GBLC). The GBLC is located about 12 miles east of Granite Falls, WA and is on the north side (right bank) of the South Fork of the Stillaguamish River (SFSR) (Figure 1 and 2). The total active area of the landslide is approximately 140 acres (566,560m^2) and consists of three distinct lobes all with steep scarps and large talus accumulations (Anchor QEA LLC, 2012; Figure 2). In the past, GBLC debris flows have affected the campground, including most recently in June 1996. In this case, sediment blocked the SFSR channel ultimately diverting the SFSR into the Gold Basin Campground and causing costly damage (Drury, 2001).

The Stillaguamish Tribe of Indians also has serious concerns regarding slope failures and erosion occurring at the GBLC. When debris flows occur, they deposit large pulses of sediment and woody debris into the SFSR. Erosion of the debris flow deposits by the SFSR coupled with sediment transport by the streams and seeps that drain the landslide produces a continual delivery of fine sediments to the SFSR (Drury, 2001). This sediment has been noted to be harmful to the salmonid species spawning grounds within the SFSR (Shannon and Wilson, 1954). Sediments will often cover salmon embryos, reducing available oxygen and suffocating them (Benda and Collins, 1992; Greig et al., 2005). Moreover, debris flows can scour riverbeds removing important gravels for spawning and riparian vegetation that help control water temperatures favorable to spawning (Pollock et al., 2009). These impacts reduce the presence of salmonid species in the SFSR; in turn reducing fish

catches for the public and for the Stillaguamish Tribe of Indians who depend upon these fish as part of their annual food supply.

At this time little is known in terms of specific rates and volume of erosion. The goals of this investigation were to 1) characterize site-specific stratigraphy and mass wasting processes, 2) to use terrestrial (ground-based) LiDAR scanning (TLS) to quantify volumes of eroded sediment within the GBLC to link it with sediment contribution to the SFSR and 3) lay the groundwork for future, long-term monitoring studies. The data and findings from this investigation will be submitted to the USFS, the Stillaguamish Tribe of Indians, and supporting consulting firms in an effort to aid decisions made by the Forest Service with regard to reopening the campground. In addition, this information might also prove useful to the Stillaguamish Tribe, who depend heavily on the SFSR for food, recreation, agriculture and residential living.

2.0 Scope of Work

The experimental setup for this investigation was designed to characterize erosional processes of the GBLC and determine within a six month period where the majority of erosion was occurring. Due to limitations in accessing the GBLC and visibility constrictions of the GBLC from the surrounding landscapes, I focused this investigation on the northeast corner of the headwall within Lobe 2 (Figure 2 – see Background for site specifics). I performed TLS scans at three different time periods (referred to as "epochs" from here on out), July 19, 2015 (epoch1), September 19, 2015 (epoch2) and January 10, 2016 (epoch3). These scans were performed at a resolutions of 15cm (epoch1) and 7cm (epoch2 and epoch3) from distances of 1.1km and 1.2km, respectively. I used these resolutions based upon my desire to capture mass wasting on a meter scale (Buckley et al., 2008; Shilpakar et al., 2016). Lower resolutions would not produce the desired resolution, yet any higher resolution would provide very large data sets causing slower processing speeds and too much detail for this study. Post processing of the data was performed within the

ESS labs at the University of Washington using RiSCAN and ENVI software programs.

In addition to TLS I performed geologic field investigations during September 2015. I did this to assign engineering classifications to the recessional outwash deposits (Tabor et al, 2002) of the GBLC. Two days of site specific field investigations were performed in teams primarily within the drainage basin of Lobe 2. I collected samples of both fine and coarse-grained unconsolidated deposits, along with their location and elevation using a Global Positioning System (GPS). I analyzed these samples in the ESS labs at the University of Washington using field methodologies outlined by the Unified Soil Classification System (ASTM, 2009). From field observations and laboratory tests, I constructed a generalized stratigraphic column. Though this stratigraphic column is not constrained by lithologic contacts due to the limited, reconnaissance nature of the field mapping, it provides a generalized section of the alternating outwash sequences within the GBLC.

The study area for this investigation is and will continue to be an area of interest for multiple parties including the USFS and Stillaguamish Tribe of Indians. Therefore it is important to provide a framework for future studies. Information such as latitude and longitude of scanning locations, resolution parameters, feasibility, and areas of interest were recorded and are provided in Appendix B. Future studies should focus on the same areas of the GBLC that were examined in this study, but may also be expanded into the neighboring lobes (i.e. Lobe 1 and Lobe 3; Figure 2). It may also be beneficial to incorporate information as to where the eroded sediment is being deposited, locations of in-situ contacts between glacial units, and sediment delivery to the SFSR.

3.0 Background

3.1 Geologic Setting

The GBLC, which lies within the Stillaguamish Watershed along the South Fork of the Stillaguamish River (SFSR) (Figure 1, Figure 2), is composed primarily of glacially deposited sands and silts that are stratified both vertically and laterally (Booth, 1989; Drury, 2001; Benda and Collins, 1992). During the late-Pleistocene, the Cordilleran ice-sheet moved south through the Puget Lowlands choking the mouth of the local valley causing an embankment of fluvial materials (Booth, 1986). These deposits formed near active or stagnant ice margins where meltwater streams deposited the sand and gravels, and the silts and clays were deposited into lakes formed by ice dams (Booth, 1986; Benda and Collins, 1992).

The GBLC can be subdivided into three distinct drainages or lobes of gravel, sand, silt and clay deposits (Figure 2). Each lobe has distinct headwalls that are eroding and transporting sediment (Drury, 2001). Groundwater flow patterns through GBLC deposits are complex and unpredictable due to spatial heterogeneity of the stratigraphy (Miller, 1999) and are highly constrained due to the steep, convergent topography. These factors cause the deposits in these lobes to be near saturated typically during rainy seasons (Minder et al., 2009). At the base of the GBLC, the SFSR is actively incising cutbanks (Drury, 2001), which in turn drives repeated mass wasting events. Recurring mass wasting at this site is also thought to relate the presence of high plasticity silts and clays within the GBLC (Shannon and Wilson, 1954).

3.2 Site Significance and Previous Studies

The high volume of fine grained deposits within the GBLC make it one of the biggest contributors to sediment within the Stillaguamish River (Benda and Collins, 1992; Drury 2001; Purser et al., 2009). For the past fifty years, the Stillaguamish Tribe of Indians has invested time and money into researching options to reduce the

sediment delivered to the SFSR. This sediment is a contributing factor to decreased salmonid spawning grounds, in turn reducing the overall population within the Stillaguamish River. In addition to the sediment being delivered to the river, the active hillslope will continue to keep the United States Forest Service (USFS) campground closed until the GBLC has been safely mitigated. The closure has affected the funding of the USFS as well as the local economy, reducing the number of visitors to the local businesses in this rural community.

As a result of the long term instability and regional importance of the GBLC to the Forest Service and Stillaguamish Tribes, many previous geologic investigations have been conducted in and around this area (Drury 2001; Anchor QEA LLC, 2012; Purser et al., 2009; Benda and Collins, 1992; Miller, 1999; Shannon and Wilson, 1954). Shannon and Wilson Inc. produced an early report in 1954 on a landslide that occurred at the GBLC. According to the report, the slide was attributed to the South Fork of the Stillaguamish River (SFSR) eroding the northern bank (right bank). Unconfined compressive strengths were determined to be 5 to 10 tons per square foot for two silt/clay specimens. Likewise, Atterberg Limit Tests were also performed. From these tests, Shannon and Wilson (1954) determined that materials underlying the region were highly plastic clays and low plasticity silts. They also concluded that many of the fine grained deposits failed in "block" form while sands and gravels tended to "ravel" down slope. The blocks failed due to shrinking and swelling effects of the silts and clays during seasonal variability (Shannon and Wilson, 1954).

In 1992, Benda and Collins performed a slope stability investigation of the Crown Pacific Property in the SRSR basin. This investigation was performed to assess slope stability for a forest practice proposed by the Crown Pacific Corporation (Benda and Collins, 1992), just west of GBLC (Figure 2). The study reported that the steep slopes and the high concentration of clays lead to debris flows in the GBLC and surrounding hillsides. These debris flows are the main mechanisms that transport sediment to the SFSR. Benda and Collins (1992) also

estimated that the GBLC contributed 25% of the annual sediment yield for the SFSR, which produces 160,000 tons/year, which equates to a contribution of about 40,000 tons of sediment to the SFSR every year.

Local geomorphologist, Dan Miller, prepared a brief report in 1999 on both the Hazel Landslide (site of the 2014 Oso, WA landslide; Figure 1) and the GBLC. Miller concluded that the sediments within the GBLC were heterogeneous and often varied throughout the complex both laterally and vertically, leading to concentrated groundwater flow in localized areas. This concentrated flow of groundwater leads to ideal conditions for groundwater to perch through the juxtaposed permeable and impermeable deposits (Miller, 1999). Lubrication of these impermeable silt and clay beds can in turn lead to failure of the overlying sands and gravels. Miller (1999) concluded there are three major mechanisms for sediment delivery to the SFSR: 1) debris flows from the GBLC that flow directly into the river, 2) erosion of exposed headwalls and previous landslide debris deposits by SFSR tributary channels draining each sub-basin, and 3) local hillslope erosion of the debris fans near the SFSR.

In 2001, Tracy Drury of GeoEngineers, Inc. provided a remediation feasibility study of the GBLC for the Stillaguamish Tribe of Indians. His report focused primarily on the sediment being added to the SFSR as a result of mass wasting of the GBLC. The addition of sediment from the GBLC has been occurring for decades and is extremely harmful to ecological productivity within the river. In a follow up to the Drury (2001) report, Anchor QEA LLC prepared a report both for the Stillaguamish Tribe of Indians and USFS. The objective of this report was to supply feasible alternatives that could implement the reduction of sediment to the SFSR, encroachment of the SFSR into the debris apron of the GBLC, and/or catastrophic damage to the Gold Basin Campground. Due to the complex terrain and high relief of the GBLC, Anchor QEA LLC focused its mitigation options on stabilizing the toes or debris fans of the GBLC rather than headwalls. The report concluded that there were five feasible options: 1) perform no action and allow natural processes to continue,

2) plant vegetation throughout the basin, 3) plant vegetation throughout the basin and construct sediment basins along the GLBC drainages, 4) completely abandon the campground and relocate the SFSR channel, or 5) vegetate the basins while diverting the drainages with a live crib wall. As of the writing of this investigation, it is unclear which option the Stillaguamish Tribe of Indians or USFS plans to use.

The Surface Water Management Department of the Snohomish County Public Works published a report in 2009 that focused on the primary sources of fine sediment in the South Fork of the Stillaguamish River (SFSR). The study took TSS (total suspended solids) measurements at different locations along the SFSR over a period of three years. From this report it was determined that much, but not all, fine sediments intruding redds (salmon spawning nests) is delivered from sources within the Gold Basin subbasin of the SFSR, most likely due to incision of the depositional fan and native materials at the GBLC (Purser et al., 2009).

3.3 Applications of Terrestrial LiDAR

Terrestrial LiDAR is a tool quickly becoming common in the offices of government agencies, consulting firms, and universities. Though terrestrial LiDAR systems cost hundreds of thousands of dollars, applications of this technology are relevant to many subjects including geology, forestry, and climate sciences. The convenience and ease at which it can be operated made it a viable tool for this investigation. TLS has been used over the past two decades to perform many earth science studies including but not limited to: monitoring sea cliff retreat (e.g. Katz and Mushkin, 2013), investigating landslide mechanisms (e.g. Collins et al., 2007), stratigraphic modeling (e.g. Bellian et al., 2005), and monitoring transportation corridors for rock movement, kinematic analysis, and structural identification while attached to a pick-up truck (e.g. Lato et al., 2009; Dunning et al., 2009). It has also been noted to be very useful in estimating volume losses and gains (e.g., Katz and Mushkin, 2013; Jaboyedoff et al., 2012; Ghuffar et al., 2013; Abellan et al., 2010; Rengers et al., 2015).

One of the main draws to incorporating TLS technology into a study is that the instruments are easy to transport, assemble, and use. They tend to weigh 5-20kg, allowing users to carry them into rough terrain. Scanners can be fully set up in areas as small as a 3m x 3m, making it possible to scan in even the tightest of environments, including transportation corridors. The effective range of a scanner is highly dependent on the model, but typically ranges from 0.1-5km (Shilpakar et al., 2016; Reigl, 2015). The TLS completes a scan by emitting a pulse of monochromatic radiation (laser) that is returned after it is reflected off various objects (ground surface, vegetation, man-made constructions, etc.), measuring a terrain profile (Petrie and Toth, 2008; Jaboyedoff et al., 2012). Deflection of the laser pulse using a system of rotating mirrors on one or more axes, or a motorized sensor lead, provide horizontal and vertical angular components (Buckley et al., 2008). Depending on the desired resolution, most scans can be completed in less than an hour. In that time, the instrument acquires a 3D point cloud, high-resolution color images, and can tie the point cloud to any previous scans that might be part of the study. The 3D point cloud typically consists of a group of several million data points with an X, Y, and Z coordinate and is the raw "product" of scanning (Buckley et al., 2008). These 3D point clouds can be captured at a higher resolution than most aerial LiDAR scans (cm scale vs. meter scale).

TLS allows frequent, accurate, and continuous monitoring of earth's surface (Jaboyedoff et al., 2012), and enables users to perform investigations from a safe distance while gathering data on unstable landforms or along highways or interstates. Closing transportation corridors, beaches, parks, or businesses to perform investigations takes time and money (Lato et al., 2009). This innovative technology has allowed government entities, consultants, and academic institutions to acquire data of earth movement within days or even hours of an event, while also allowing long term monitoring (e.g. Rohrbaugh, 2015; Ghuffar et al., 2013; Abellan et al., 2010; Collins et al., 2007; Rengers et al., 2015; Harpold et al., 2015; Rengers et al., 2016).

4.0 Methods

4.1 Field Methods

4.1.1 TLS Field Operations

Site selection and coverage is one of the most important factors to consider when setting up a TLS study as it allows the maximum coverage of the study area (Buckley et al., 2008). Reduction in the line of site to the target will cause increased data gaps due to laser interception by foreign objects or landforms. Data gaps are places within the scans that do not return any information. This usually occurs due to an obstruction within the line of site or factors such as atmospheric moisture, snow, and vegetation.

Prior to conducting any TLS scans of the GBLC, I conducted four reconnaissance trips to the Mt. Baker-Snoqualmie National Forest in order to discern the best views of the slope failure. I attempted to avoid as much vegetation as possible while being close enough to the site (4 km or less – the range of the TLS instrument) to generate complete scans. I ultimately chose two sites to perform scans, both on the left bank (south side) of the South Fork of the Stillaguamish River (Figure 2), as they provided the most data given the environmental limitations (i.e. vegetation, slope aspect, etc.). From these locations, I scanned a majority of Lobe 2, with the exception of the eastern wall and the extensive talus apron. I used the Trimble GEO 7x GPS to georeference the locations of the scanner so that relocation was possible when conducting succeeding scans during subsequent epochs.

When conducting the TLS scans, I used the Riegl VZ 4000 (hereafter referred to as VZ 4000) to generate 3D point clouds of the GBLC. The VZ 4000 has the ability to collect measurements at 50 kHz laser pulse repetition rate, with a precision of 10mm, and an accuracy of 15mm at up to approximately 4000m radial distance from the scanner lens to the target surface (Riegl, 2015). The VZ 4000 (Figure 3) has the ability to perform a 360° scan about a vertical axis (yaw) with a ±30° vertical

window from horizontal (pitch). To begin each epoch, I created a new project file and then entered the scan positions (ScanPos001 or ScanPos002) into the RiSCAN software as needed within a given project (epoch). At each scan position I conducted a preliminary low resolution (150cm) panorama (360° yaw; +30°, -30° pitch) scan. Upon completion of the low resolution scan, the VZ 4000 used a fully calibrated Nikon D800 36MP camera that was mounted on the scanner to acquire high resolution image mosaics. The mosaics are automatically registered to the laser point cloud. This functionality provided both a detailed gigapan-like image for the survey area that could be draped over the derived topography, and automatically assign RGB color to each point. This in turn complimented the recorded IR (infrared) laser intensity values. These complementary data were useful for data analysis and interpretation during post-processing when direct field observations were not possible.

Following the preliminary low resolution scan, a high resolution scan (15cm for epoch1, 7-8cm for epochs2 and 3) was performed for each epoch. Scan resolution was chosen based on the work of Shilpakar et al. (2016) who performed repeat scans using three different TLS machines at two different study areas. Shilpakar et al. (2016) performed one study using the same scanner to perform three scans from different locations over ten different time periods (epochs). The second study was performed using two different scanners. These two scanners performed data acquisition from three different locations at two different time intervals. From these repeats scans, it was determined that the object of the study and distance from the object were the biggest factors that affected resolution choice.

Prior to collection of the high resolution scan, I reviewed the 360° panorama scan data in RiSCAN to determine where to focus the high resolution scan. In addition to considering site visibility, it was also important to consider the limitations of the maximum pitch above horizontal when scanning the steep escarpment, as the scanner could not reach the top of the slope when too close.

After I completed the low resolution, panoramic and high resolution, user-parameterized scans at a given scan position, the data were reviewed for errors (i.e. missing data, gaps in the data, and/or poor returns, etc.). Assuming no errors, the equipment was then transported to the next scan position to repeat the previous steps, still within the given epoch. Once I had completed both low and high resolution scans at each scan position, the data were saved and transferred to an external hard drive for redundancy and post processing.

4.1.2 Field Investigations and Sample Collection

I directed two days of site specific field investigation along the headwall and talus apron within the drainage basin of Lobe 2. For the first day, I brought out a team of two graduate students from the University of Washington, while the second day I led a team of three students. We used a Trimble Geo 7X GPS unit (Trimble) to mark the locations of all field sites where samples were collected (Figure 4), with two samples being collected at site GBLC-2G due to the clear homogeneous contact between beds of sand and gravel at this location. In order to determine the engineering characteristics, we recorded properties such as plasticity and dilatancy at the locations where fine-grained samples were collected. Dilatancy was determined by creating a saturated sample in the palm of the hand that was then tapped approximately ten times. If water rose to the surface in a few taps, the sample was considered to have rapid dilatancy. If it had a small amount of water rise, it was considered to have low dilatancy. If no water was present it was classified as having no dilatancy. For plasticity, a sample was rolled into a 3mm thread. This step was repeated until a thread could no longer be rolled. Samples were described as having low, medium, or high plasticity based on the number of times it could be rolled into a 3mm thread. For all the samples, we described their color, moisture content, sedimentary structures, visible grain size information, and any other significant characteristics. All samples were bagged and brought back to the ESS labs for further classification and analysis.

4.2 Lab Methods

4.2.1 TLS Post-processing in RiSCAN and ENVI Software

I used RiSCAN and ENVI software programs to determine the volume of sediment eroded from the northeast headwall of Lobe 2 within the GBLC between July 2015 and January 2016 (Figure 2). RiSCAN is the proprietary Reigl software for acquiring, processing, and handling the data from Reigl scanners. It was used to visualize the amount of sediment loss in X (east-west), Y (elevation/vertical), and Z (north-south) planes. Though there are many software programs that can be used for measuring volumes, ENVI was used due to its availability at the University of Washington, along with access to training materials such as manuals, labs, and colleagues. ENVI has been used in past studies to determine changes in tree canopies, changes in shoreline morphology, and differences in ambient air temperatures (e.g., Mikhail and Rachold, 1999; Jusoff, 2008; Jusuf, 2007). Once the area of interest was analyzed in RiSCAN the actual volumes of sediment lost were calculated in ENVI.

In order to address occlusion issues due to line of sight limitations, each epoch consisted of two scan positions that had to be co-registered into the same coordinate system. I used multiple large tree stumps along the headwall of Lobe 2 to co-register the two scan positions with each other. I assigned these tree stumps a "registration point" correlating the same tree stumps in each of the two scans (Figure 5). Once complete the scans were combined to produce both a color and a black and white hillshade (Figure 6).

After registering the data from the two scan positions of each epoch in a unified point cloud, the data were inspected for irrelevant objects such as trees, rivers, and surrounding topography for each epoch separately. By removing unneeded point cloud data I reduced the amount of time needed to process the data by decreasing the file size. Next I ran a surface comparison in RiSCAN between

successive epochs to view the surface changes in the X, Y, and Z coordinates planes. To accomplish this I first triangulated the point cloud data for each epoch to create a surface instead of a point cloud. By triangulating the data I created planes between points, (a mesh), yielding a 3D surface model, rather than a point cloud. After I created the mesh for one epoch, I co-registered it with the point cloud of another epoch using the same technique with the tree stumps, as outlined above. Once all epochs were co-registered I performed the surface comparison in the XY, XZ, and YZ planes (Figure 7 and 8). By creating these comparisons I could visually assess areas along Lobe 2 that sustained vertical and/or horizontal changes.

While performing the surface comparison in RiSCAN I noted areas of interest along the XZ plane so that I could calculate volume changes in ENVI. An area of interest had to be identified on the XZ plane in RiSCAN because when the data are exported into ENVI, the data is viewed in 2D from a "birds-eye" view (i.e. the X and Z plane in RiSCAN). Once I identified an area of interest I outlined it in ENVI to calculate the amount of lost or gained sediment between epochs. To accomplish this, I first had to export each epoch point cloud data from the comparisons made in RiSCAN to ENVI. Once imported to ENVI, I converted the vector data (point cloud) into raster data (digital elevation model – DEM). In ENVI, the X and Y coordinates are represented as pixels measured in meters (m). I used a pixel size of 0.3m for both the X and Y coordinates. This allowed me to have at least four points from the point cloud data in each pixel. These numbers were chosen because any smaller pixels caused errors within ENVI, while larger pixels were too coarse for the desired detail in this investigation (i.e. meter scale). With these specified parameters, I created a digital elevation model (DEM) of both epochs in ENVI.

After I created the two DEMs in ENVI, I utilized ENVI's change detection tool to produce a change map of topography DEM, where volume lost or gained is displayed (Figure 9). This is similar to the images I created in RiSCAN, except presented in "bird's-eye" view, which is preferred.

4.2.2 Soil Sample Classification

During my two days of site specific field investigations, I collected seven samples for further analysis in ESS Labs at the University of Washington. I obtained the seven samples from sites GBLC-1B, GBLC-1C, GBLC-1E, GBLC-2E, GBLC-2G (x2), and GBLC-2J (Figure 4). Three of the samples were fine grained, whereas the other four samples were coarse grained. I dried all seven samples in an oven at 110°C for twenty-four hours. I did this to dry the coarse grained samples and determine the dry strength for each of the three fine-grained samples, as outlined by the Unified Soil Classification System (ASTM, 2009). This information combined with the characteristics determined in the field allowed me to assign an engineering classification to each sample.

For the four coarse grained samples, I performed a grain-size analysis to determine the percent of fines, sands, and gravels. I used the following sieve sizes to complete the analysis: no. 4, 10, 20, 40, 80, 200 and 5/8in. The sample was weighed and then poured into the sieves. The sieves were placed in a mechanical sieve shaker and shaken for 10 minutes. After the shaking was complete, I removed each sieve one by one and weighed the remaining materials in that sieve. After all the sieves were weighed with their respective materials, I recorded the final weight of the original container with the entire sample (Appendix A). I recorded the percent passing {(weight on sieve(s)/total weight) x 100} and percent retained {(weight remaining in sieves/total weight) x 100}. I also determined the individual percentages of grain-sizes. I plotted the data on grain size distribution charts with the grain size on the x-axis and the percent (%) passing on the y-axis. I compared the results to the Unified Soil Classification System (ASTM, 2009) chart and classified them according to their percentage of fines, sands, and gravels. I determined the coefficient of uniformity (Cu = $\frac{D_{60}}{D_{10}}$) and coefficient of concavity (Cc= $\frac{D^2{}_{30}}{D_{10}D_{60}}$) after the samples were plotted on the grain size distribution charts.

Using the results from this analysis, I assigned engineering classification to each of the samples.

5.0 Assumptions and Limitations

5.1 Hardware and Software

The VZ 4000 is a complex machine that has many variables that can be changed prior to or during a scan. Factors such as atmospheric conditions and scan parameters can yield errors when capturing the data. For example, if the atmospheric conditions are out of the specs provided by the manufacture, it has the potential to malfunction or seize working altogether. The speed at which the VZ-4000 is assigned to scan at, can also have an effect on the data. If the VZ-4000 is set to scan at a higher speed (e.g., 150 kHz, 300 kHz, etc.) it reduces the range at which you can scan, which can cause a gap in the data (Reigl, 2015). However, if you slow it down (e.g., 30 kHz), it can take more time to complete the scan, but the data files become very large, slowing down post-process review of the data.

During the post-processing of the GBLC data there are many factors that can be adjusted within the software programs in order to perform the volume calculations. Factors such as resolution, triangulation, and pixel size can have an effect on the results. When comparing scans of different resolutions it is possible that one epoch will have more data gaps than the other, which may provide more coverage of one epoch, but not the other. When triangulating the data into a mesh, there is the option to choose the spacing between the points that are to be connected. A larger spacing can connect more point data but tends to lose detail in the topography. Too small of a spacing can create gaps in the mesh, increasing data gaps when doing the surface comparison. Similarly, when choosing a pixel size in ENVI, having too big of a pixel size would not supply enough point data, yet too small of a pixel would yield no results.

5.2 Line of Sight

One of the most difficult issues I faced during field reconnaissance was determining which locations to use for data collection. The GBLC resides in the Mt. Baker-Snoqualmie National Forest, and consists of both young and old growth vegetation, much of which has not been altered by human interactions. Due to the heavy vegetation there were few locations around the GBLC that had a direct line of sight into any of the three lobes. The locations I selected for data collection had the best view of Lobe 2. This is one of the main reasons I focused this investigation on the northeast headwall of Lobe 2. I was unable to collect data from any of the other lobes due to vegetation interfering with the line of sight from the VZ 4000. The eastern zone of failure of Lobe 2 was also negated for the same reasons.

5.3 Climate Variability

Water moisture in the air can be a source of feedback and error when it comes to TLS, reducing maximum range and interfering with the laser returns (Buckley et al., 2008; Boehler et al., 2003). Fortunately, during the scanning of epoch1 (July 2015) and epoch3 (January 2016), the weather was relatively clear with sunshine. These conditions are ideal because there is little chance for interference with the lasers from the VZ 4000. During the scanning of epoch2 (September 2015), the weather alternated between dry, foggy, cloudy, and raining. The times with heavy fog or rain, the scanner picked up additional "noise" or feedback from the VZ 4000's lasers reflecting off of moisture in the air. This causes extra data points to cloud the data set making it difficult to view and manipulate. It is not uncommon to have reflections in the data due to moisture in the atmosphere (Collins et al., 2007). Fortunately, I was able to gather data for epoch2 during a few rare instances when moisture was absent. Similarly to epoch2, I noticed some data gaps in the epoch3 point cloud due to snow appearing on locations (mostly benches) within the Lobe 2 drainage (Figure 10). Though I do not believe this affected the overall results substantially, it should be noted snow caused data gaps on some of the GBLC's benches.

5.4 Sample Collection

As this is a landslide complex, many portions of the slide are or have been recently mobile. Therefore, my colleagues and I attempted to collect samples that to the best of our knowledge were in place. We looked for outcrops that appeared to be part of the in-situ walls and did not show signs of slumping, rotation, or sloughing. We used a small hand scraper to clear away any loose material, then a shovel to remove the sediment samples from the outcrop. The exact location at which the samples were collected may have had slight errors as well. The potential error in location could be up to 0.5m in places due to line of sight issues between the Trimble and the satellites.

5.5 Sediment Delivery

In section 7.2 I discuss the potential contribution of sediment from the GBLC to the South Fork of the Stillaguamish River (SFSR). In these calculations I am assuming that the entire mass of eroded sediment recorded from this investigation has been added to the SFSR and thus, the estimate serves as a maximum contribution from lobe 2. This is assumed because there is no evidence of the locations in which this sediment was deposited. Also, due to the limited information on the discharges within the SFSR, I assume an average discharge during the time of this investigation, even though different climate conditions during this time most likely varied the discharge values. When calculating TSS (total suspended solids) I assume an average density of 2.65 g/cm^3 based on the work of Koloski et al. (1989) and Savage et al. (2000).

6.0 Results

6.1 Field Observations

During my two days of site specific field mapping and characterization I observed and recorded processes occurring within and around Lobe 2 of the GBLC. This included actively eroding landforms, geologic deposits, stratigraphic

orientations, and running water. Along the right bank of the South Fork of the Stillaguamish River (SFSR), I observed younger vegetation consisting primarily of alder trees. These trees are sitting on top of a hummocky chaotic deposit that contained large tree trunks/branches, water seeps, and multiple grain sizes including boulders (Figure 11). Based on analysis of aerial LiDAR imagery, this landform appears to be deposits from previous GBLC mass wasting events (Figure 4).

Upslope, on Lobe 2 of the GBLC itself, I observed large, mostly vertical exposures some over 50m tall, consisting of alternating beds of gravels, sands, silts, and clays. Near the headwall, within 5 to 10 meters of the top of the hillslope, slopes were vertical. These vertical sections were observed to be unstable, with constant raveling sands and gravels capped by what appeared to be a 1m thick section of glacial till. My team and I also heard and saw noticeable ravels occurring all around the drainage of Lobe 2. Furthermore, I observed at least two areas along the eastern wall that had blocks of silts and clays shear off of the walls (Figure 12). I inferred that these were the most common types of erosion occurring within Lobe 2 as the talus piles near the headwall appeared to be made of large blocks of silts and clays covered in sands and gravels.

6.2 Soil Sample Classifications

Based on field observations, grain size distribution charts (Figure 13-16), and for fine-grained samples, dry strength tests, I determined that the GBLC is composed of alternating poorly-sorted sands and gravels with thick sections of high plasticity clays and silts. The lower elevations of the GBLC consist mostly of thickly-bedded, poorly-sorted sands and gravels. At around 400m in elevation, there is a 50m section that consists of high plasticity clays and silts. These clays and silts typically alternate and are interbedded with gravels and sands in places. On top of these silts and clays is a very dense section of interbedded, poorly-sorted sands and gravels. Table 1 shows the classifications I determined using the methods outlined in section 4.2.2. In Figure 17 and 18, I compiled this information, providing a

generalized stratigraphic column that shows the relationships between collected samples.

Table 1 - Sample names, classifications, and descriptions from field investigations at all six locations.

	Sample Name	Unified Soil Classification	Sample Description	Coefficient of Uniformity (Cu)	Coefficient of Concavity (Cc)
Coarse Grained	**GBLC-1E**	SP	Loose, wet, dark brown to grey, alternating beds of sand and gravel throughout outcrop. Poorly graded sand with gravel.	5.3	0.85
	GBLC-2G (Gravel)	GP	Very dense, wet, dark brown to tan, thickly bedded sands and gravels. Poorly graded gravel with sand and trace cobbles.	38.9	19.8
	GBLC-2G (Sand)	SP	Very dense, wet, dark brown to tan, thickly bedded sands and gravels. Slightly gravely sand.	6	0.66
	GBLC-2J	SP	Very dense, wet, dark grey, interbedded sands and gravels with intermittent laminae of silts and clays, signs of oxidation apparent. Slightly silty fine sand.	6.4	0.81
Fine Grained	**GBLC-1B**	CH	Very stiff to hard, dark grey, perching water, barely indent with finger, high plasticity, blocky, bedded silts and clays.	N/A	N/A
	GBLC-1C	CH	Very dense, dark and light grey, barely penetrates with thumbnail, high plasticity, bedded with alternating laminae.	N/A	N/A
	GBLC-2E	MH	Dense, light grey, barely penetrates with thumbnail, medium to high plasticity, bedded to thinly bedded silts and clays.	N/A	N/A

6.3 Spatial Patterns

Using RiSCAN software, I located an area of interest near the northeast headwall on Lobe 2 by looking at the surface comparisons between epochs as outlined in Section 4.2.1. By co-registering the two scan positions from each epoch, I

was able to compare each epoch's point cloud. This produced 3D images of areas that sustained erosion from epoch1 (July 2015) to epoch2 (September 2015), epoch2 (September 2015) to epoch3 (January 2016), and also from epoch1 (July 2015) to epoch3 (January 2016). Results were only interpreted near the northeast corner of Lobe 2 as it contained the fewest data gaps and lacked significant vegetation.

Results showed a loss of ~1-2m in the vertical and cliff-normal plane along the northeast headwall between epoch1 and epoch2. I used trees as traceable markers, and within this time interval there were no noticeable trees observed within the talus slope of Lobe 2. Between the time period of epoch2 and epoch3 there was 10's of meters of erosion near the eastern portion of the northeast headwall both in the vertical and cliff-normal directions. The coordinate direction that sustained the most erosion occurred in the vertical plane (Figure 7). This is most likely due to a large portion of the headwall eroding back into the hillside to the north. RiSCAN comparisons show as much as 15m of vertical drop near the northeast corner of Lobe 2 (Figure 2 and 7). Similarly, there is evidence of up to 20m of headwall retreat in the cliff-normal plane (Figure 7). Furthermore, I found ~1-5m of erosion in other locations along the headwall and within the drainage basin during the time between epoch2 and epoch3 (Figure 8).

When I compare the results from epoch1 to epoch2, to that of epoch2 to epoch3, it is apparent that more erosion occurred after the scanning of epoch2 (September). This is seen in the data as an increase of ~1600% in sediment eroded. It should be noted that there was an extra 112 days between epoch2 and epoch3 compared to that of epoch1 to epoch2.

Despite obvious erosion, no deposition of sediment was detected in any region of the scanned site, including within the talus apron through the entirety of the study. Though the data did not show deposition of sediment, evidence of mobile trees and tree stumps exist below the headwall. The addition of these trees and tree

stumps were represented by added volume within the RiSCAN surface comparison in epoch3 (see section 6.4 below; Figures 7, 8, and 19).

6.4 Calculated volumes

Using the digital elevation models (DEMs) created in ENVI, I calculated volumes of erosion for epoch1 to epoch2, epoch2 to epoch3, and epoch1 to epoch3. With predetermined values for the X and Y coordinates (0.3m), I used ENVI to obtain the Z coordinate (m) and the total area in which to calculate the volume. I found that between epoch1 (July 2015) and epoch2 (September 2015) there was 238m^3 of material eroded from the northeast corner of the GBLC (Table 2). Between epoch2 (September 2015) and epoch3 (January 2016), 3,873m^3 of material was eroded. During the entirety of this investigation (i.e. epoch1 to epoch3) a total of 4,767m^3 of sediment was calculated to have eroded from the northeast headwall (Table 2). This is a different result than the sum of the first two time intervals, which totals 4,111m^3 (238m^3 + 3,873m^3).

Table 2 - The values used to calculate volumes differences between each epoch. The changes in volumes include a possible error of 30%.

Epoch Comparison	X-Coordinate	Y-Coordinate	Average value of pixels (m)*	# of Pixels	Change in Volume (± error of 30%)
Epoch1 (July 2015) - Epoch2 (September 2015)	0.3m	0.3m	-0.036m	69686	-238m^3
Epoch2 (September 2015) - Epoch3 (January 2016)	0.3m	0.3m	-0.757m	69699	-3,874m^3
Epoch1 (July 2015) - Epoch3 (January 2016)	0.3m	0.3m	-0.611m	70564	-4,767m^3

**elevation difference in the Z - direction*

7.0 Discussion

This investigation, which was conducted over a six month period (July 19, 2015 to January 10, 2016), accomplished three goals: 1) characterized site-specific stratigraphy and mass wasting processes, 2) used TLS to quantify volumes of eroded sediment within the GBLC to link it with sediment contribution to the SFSR and 3) laid the groundwork for future, long-term monitoring studies. I will discuss the results and implications of each of these three goals in the sections below.

7.1 Geologic Interpretation

My two days of site specific field investigations revealed that Lobe 2 of the GBLC consists of unconsolidated glacial outwash deposits that vary both laterally and vertically. This is important information relevant to interpreting erosional processes. Knowing that that there are impermeable deposits (silts and clays) underlying permeable deposits (gravels and sands) is bound to perch groundwater in many locations throughout the GBLC. This perched ground water can cause many lubricated surfaces allowing the overlying sands and gravels to slough, ravel, and slide off of these impermeable deposits, while also increasing pore fluid pressure, decreasing the strength of the overlying materials, leading to failure. Similarly, perched water can slowly percolate into the silts and clays causing them to shrink and swell with alternating seasons, leading to block or slab failures as Shannon and Wilson (1954) pointed out. This is most likely the primary failure mechanism, as I determined that the silts and clays within Lobe 2 were typically highly plastic.

I interpret that the sediments within Lobe 2 of the GBLC were deposited as part of an ice-contact margin. I reached this conclusion due to alternating dark grey to light grey laminae in the clay and silt deposits, which are indicative of seasonal variability in glaciolacustrine deposits (Shaw et al., 1978). This conclusion supports earlier work by Booth (1986), who concluded that the valley in which this

investigation took place was once dammed by an ice sheet to the west near the opening of the valley. Structures, such as cross-bedding and ripple marks, found within the GBLC deposits also indicated that this was a fluvial environment.

7.2 TLS Erosion Volumes and the Impact of Precipitation

The results from this investigation confirm that the Gold Basin Landslide Complex (GBLC) is consistently and actively eroding (Shannon and Wilson, 1954; Benda and Collins, 1992; Miller, 1999; Drury, 2001; Anchor QEA LLC, 2012). My preliminary estimates of erosion show that in a period of six months there was a loss of ~4,800m^3 from the northeast headwall within Lobe 2. This estimate does not include sediments that have eroded from other locations within Lobe 2, so this is a minimum erosion volume for the period of July 2015 to January 2016. Surface comparisons done using the RiSCAN software revealed that there was as much as 20m of headwall retreat in the northeast corner of Lobe 2, which suggests a very unstable hillslope and that the total erosion volume estimates are not unreasonable.

Ideally, when calculating volumes with TLS, the project area should be compared to an area that remained stable throughout the study in order to determine the uncertainties, especially error that results from post-processing the data (e.g Katz and Mushkin, 2013; Shilpakar et al., 2016). Unfortunately, during this study I was unable to locate an area that did not experience erosion or deposition; therefore I could not attribute an exact amount of error to the process. In previous investigations where TLS was used to calculate erosion and depositional volumes in landslide mapping and monitoring, researchers found errors ranged from 1-10cm, usually increasing with distance (e.g. Katz and Mushkin, 2013; e.g. Jaboyedoff et al., 2012; e.g. Collins et al., 2007, Shilpakar et al., 2016). Therefore, in this investigation I assume an uncertainty of 30% (Table 2) for the sediment volumes calculated. With a volume of 238m^3 between epoch1 and 2, and a volume of 3,873m^3 for epoch2 to 3 there should be a total volume of ~4,100m^3. Yet when I calculated the erosion volume for epoch1 to epoch3 I received a number of ~4,800m^3. If we apply the 30% error, the gap of ~700m^3 is not unreasonable.

Between epoch2 and epoch3, TLS results revealed 25-30m of headwall retreat in the northeast corner of Lobe 2 (Figure 7 and 19). This is a large amount of retreat over a four month period, but it is on par with values estimated at the Oso WA 2014 failure site (Figure 1) by Keaton et al. (2014). Keaton et al. (2014) performed field reconnaissance and found that the scarp of the target landslide retreated approximately 3-6m in a two month period. The study site location is approximately 25km northwest of the GBLC and is subjected to similar precipitation amounts and has similar stratigraphy of alternating glacial deposits made of gravels, sands, silts, and clays (Tabor et al., 1988; Booth, 1989). During the time of the investigation by Keaton et al. (2014) the targeted landslide was free of vegetation exposing the stratigraphy, allowing direct interception of atmospheric precipitation. This is very similar to exposure presented at the GBLC.

Shipman (2001) explains that the interception of precipitation by vegetation is one of the biggest factors that prevent over saturation of soils, which is the typical driving force for landslides in Washington State. As mentioned above, the vegetation cover of the GBLC, especially that of Lobe 2, is mostly absent within the drainages and along the headwall. Between epoch2 and epoch3 the GBLC was subjected to approximately 1040mm of precipitation (41in; Table 3). With at least four instances where more than 44.45mm (1.75in) fell within a 24 hour period (Figure 20). Tubbs (1974) found that 70% of landslides in the Seattle, WA area occurred on one of three days in which precipitation exceeded 44.45mm (1.75in) in twenty-four hours. Therefore, I infer that there was potential at least four times between epoch2 and epoch3 where substantial erosion occurred. It should also be noted that this particular area of Washington State received, on average, more precipitation than average (Table 3), therefore we can infer that the erosion seen during this investigation could be more than what might be expected in the future and in past years.

Table 3: Monthly precipitation values and monthly average precipitation values for the Darrington Ranger Station, which is approximately 20km north of the GBLC (Data provided by the Western Regional Climate Center, 2016).

Year	Month	Precipitation Total (mm)	Precipitation Total (in)	Historical Averages (mm)	Historical Averages (in)
2015	July	30.73	1.21	30.86	1.21
2015	August	111	4.37	43.43	1.71
2015	September	98.55	3.88	92.46	3.64
2015	October	236.2	9.3	188.47	7.42
2015	November	367.8	14.48	295.91	11.65
2015	December	337.8	13.3	333.25	13.12
2016	January	334	13.15	302	11.89

7.3 Sediment Effects on the South Fork of the Stillaguamish River

Sediment that is <0.85mm is one of the biggest contributors to the reduction to salmonid survival (e.g. Cederhold and Salo, 1979; Chapman, 1988; NMFS, 1996; Purser et al., 2009). It tends to intrude redds (salmonid spawning nests) which in turn suffocates salmonid embryos due to reduced oxygen flow (Rhodes et al., 1994; Rhodes and Purser, 1998; Rhodes et al., 2001; Purser et al., 2009). Similarly, suspended sediments increases turbidity, which in turn impairs sight feeding and growth of salmon (Sigler et al., 1984; Lloyd et al., 1987; Purser et al., 2009). From my results and field investigations it is possible to infer that the majority of the sediment being delivered to the South Fork of the Stillaguamish River (SFSR) from the GBLC is less than the threshold of <0.85mm. From the grain size distribution charts (Figures 13 – 16) it is possible to see that the minimum percent of fines (<0.85mm) is ~10% with a maximum percent near 80%. Similarly, it has been determined from this investigation and others (e.g. Shannon and Wilson, 1954; Benda and Collins 1992; Miller, 1999; Drury, 2001; Anchor QEA LLC, 2012), that a large portion of the stratigraphy within the GBLC is composed of fine-grained deposits of silts and clays.

In a fine grain sediment study of the South Fork of the Stillaguamish River (SFSR), Purser et al. (2009) found that the GBLC was a large contributor of turbidity and fine grain sediment deliver to the SFSR. From aerial photo analysis they estimated that from 1998 – 2006 the Gold Basin Landslide contributed ~140,000m^3 of sediment to the SFSR. Over the span of three years (2007 – 2009) they took six TSS (total suspended solids) measurements upstream and downstream of the GBLC. In each sample they found there was an increase in TSS, mainly contributed by the GBLC.

Assuming all the sediment eroded between epoch2 and epoch3 was delivered to the SFSR and that discharge was generally around 295 ft^3/s, I find that the GBLC contributed a TSS of 110mg/L over the four month period. According to Lewis (1996), a TSS of over 100mg/L can impair the vision of fish within a stream. On December 12, 2007 Purser et al. (2009) recorded that suspended sediment upstream from the GBLC in the SFSR was approximately 20,000 kg/day, while downstream of the GBLC it was approximately 200,000 kg/day (Figure 21). Since the time period between epoch2 and epoch3 occurred during the same month, I used the TLS data to calculate the possible kg/day that the GBLC could have contributed during this time period. I find that over the 122 day period between epoch2 and epoch3 the GBLC produced approximately 80,000 kg/day from the ~3,900m^3 of eroded sediment. This amount does not include any sediment that may have been eroded from the other lobes within the GBLC, nor does it include eroded sediment outside of the area of interest within Lobe 2.

From this information I can infer that the GBLC is not only contributing large amounts of suspended sediments to the SFSR, but also that many of these sediments are small enough (<0.85mm) to interfere with spawning and feeding habits of local salmonid species. These calculations are preliminary and subject to assumptions that could lead to both under and overestimates, for example during times of heavy precipitation (epoch 2 to epoch 3) or dry periods (epoch 1 to epoch 2), respectively.

In any case, these data suggest that long-term monitoring and comparison to climate data, sediment yields in the river, and salmon population data would be valuable.

7.4 Considerations for Future Site Investigations

Firm conclusions regarding hillslope degradation, sediment aggradation, stratigraphic contacts, and erosional processes within the GBLC require long-term observations and quantification of erosion patterns and volumes. In addition, future investigations should be broadened to other parts of lobe 2 as well as the other two lobes of the GBLC if possible (Figure 2). For example, limited analysis of aerial LiDAR suggests that Lobe 3 is more susceptible to gullying and that Lobe 3 might erode into Lobe 2 (Figure 4).

My preliminary results illustrate that Lobe 2 has other areas with significant areas of erosion, including along the west headwall and benches, where meters of noticeable erosion are observed (Figure 8). It would be beneficial to see if these erosional values are consistent through time, and if the same areas continue to show retreat along the headwall. My findings show that if the headwall continues to retreat to the north, it will eventually erode into the adjacent valley, compounding sediment delivery to the base of the hillslope and possibly the South Fork Stillaguamish River.

One issue that I did not address directly in this investigation is the tracking of the eroded sediment. According to the quantitative analysis I performed on the erosion, about 4,800m^3 of sediment was removed from the northeast headwall. Yet, the VZ 4000 scans showed less than a meter of deposition over visible spectrum of the talus apron. I hypothesize that much of the sediment was either dispersed across a larger area, eroded further down the talus apron, or was delivered to the SFSR by a debris flow or fluvial processes. Future investigations should be designed to more carefully investigate both how the eroded sediment is transported and where it is deposited.

The most important modification I would suggest for future studies is to increase the frequency of scans. More frequent scans would allow a researcher to constrain times of erosion with precipitation events. In addition, future studies should continue to scan from the locations outlined in Figure 2, but should also be expanded to capture more of the GBLC. The winter months provide the best line of sight due to the lack of vegetation, however, the chances of interference from winter precipitation could cause delays or data gaps. Tools such as motion sensor cameras mounted within the lobes of the GBLC would allow erosional events to be captured when scanning and field work are not possible. This type of tool would provide insight to the erosional mechanisms of the GBLC and prevent the need to enter these hazardous terrains. Benchmarks, which would allow visual confirmation of mobile features within the GBLC useful in post-processing the data, would be beneficial if placed at a range of locations around the study site. These data would also help to determine if there is rotational, slumping, or slab movement.

With the TLS, areas of heavy erosion can be identified and quantified. Erosional maps combined with locations of permeable and impermeable contacts could lead to identifying areas of variable mechanisms of erosion if scanning is frequent. With the high resolution of the TLS it may also be possible to perform detailed geologic or stratigraphic mapping. For example in Figure 22 it is possible to see that even with the 7-8cm resolution used for this investigation, individual beds can be studied. Using this resolution or even increasing the resolution would allow studies of the stratigraphy near the unstable headwall without the potential for injury.

7.5 Data Gaps and Volume Errors

When I compared the volume quantities calculated using ENVI, I noticed a gap in the amounts calculated from epoch1 to epoch2 and epoch2 to epoch3, compared to that of epoch1 to epoch3. Ideally the differences calculated between epoch1 – epoch2 and epoch2 – epoch3 should add up to the total calculated from

epoch1 – epoch3. As shown in Table 2, this was not the case. A volume deficit of 655.1m^3 was calculated from these findings. Though it is not uncommon to have an error of 10-30% in such cases, this deficit should still be discussed. An uncertainty of 30% was assumed due to the fact that an uncertainty could not be factored as outlined in section 7.1. This deficit could be attributed to the data gaps between each scan period or the volumetric calculation process. For example, as mentioned above the hillside was much more visible during epoch3, which could have captured more of the hillside adding volume to epoch3.

When I created the polygon (Figure 9) for the volumetric calculations, I found it difficult to create the exact polygon over the same location within the three different DEM comparisons (epoch1 – epoch2, epoch2 – epoch3, epoch1 – epoch3). Table 2 shows the different quantities of points collected in each volumetric calculation. Between epoch1 – epoch2, the difference is only 13 points, but between epoch1 – epoch3, the difference is 900 points. I am unable to determine if this is contributing to the 655.1m^3 of volumetric difference.

Finally, a factor that must also be considered in the potential error of the volumetric calculations is the differences in resolutions between epoch1, epochs2, and epoch3. As noted in section 4.1.1, I used a resolution of 15cm during epoch1, but for epochs 2 and 3, I refined that to a resolution of 7-8cm. This occurred because epoch1 was considered a testing trial to see what type of resolution would be needed later. I chose a higher resolution in an effort to better co-register the tree stumps outlined in section 4.1.1. The change in resolution may play a role in the missing 655.1m^3 of sediment. However, since I used the same epoch1 data for all of the calculations, any errors from resolution would have been distributed into all of the results.

8.0 Conclusion

Terrestrial (ground-based) LiDAR (TLS) scans and site specific field investigations were used to perform volumetric analyses and assign engineering classifications to the glacial deposits within the Gold Basin Landslide Complex (GBLC). My preliminary TLS results show that ~4,800m^3 of sediment was eroded from the northeastern headwall of Lobe 2 of the GBLC over a six month period. From the analysis it is apparent that the northeast headwall is experiencing both vertical and lateral erosion into the hillside (Figure 7 and 19). This is consistent with the findings of Drury (2001), Anchor QEA LLC (2012), and Shannon and Wilson (1954). From the TLS data I could not discern if the eroded sediment reached the SFSR or if it was deposited within the talus apron. This is an important aspect that should be continually studied at the GBLC. This could be conducted with benchmarks, motion sensor cameras, or quantitatively with TLS by scanning within the drainage basins of the GBLC.

The northeast headwall is not the only part of Lobe 2 experiencing erosion; therefore, I can infer that there was a larger volume of sediment eroded than calculated for this investigation. With only three epoch scans, it is not feasible to determine a rate of retreat for the northeast headwall; however, it would be feasible if the GBLC was scanned repeatedly into the future. Continued retreat of the headwall to the north and northeast would eventually cause the GBLC to converge with the valley to the north. This in turn would cause increased sediment delivery to the SFSR. As mentioned in section 7.2 the GBLC is already contributing significant amounts of sediment to the South Fork of the Stillaguamish River (SFSR). Convergence of the two adjacent valleys would further decrease vegetation cover, increasing the chance of erosion.

From my field observations and material tests, I concluded that the stratigraphy of the GBLC consists mainly of poorly sorted sands and gravels interbedded with high plasticity silts and clays. The stratigraphic column created for

this investigation (Figure 18) shows that there are sands and gravels that overlie a thick section of silts and clays, similar to that of Benda and Collins' research (1992). According to Miller (1999) the groundwater for this area perches off of these silts and clays. My field observations confirmed these earlier findings as I witnessed seeping of perched water and conclude that this leads to focused erosion along the upper extents of the headwall.

This investigation shows that TLS is a very convenient and productive tool for monitoring eroding hillslopes. With continued TLS scanning, seasonal, yearly, and even decadal erosion rates and sediment flux maps could be determined for the GBLC. Despite factors such as human error, precipitation, vegetation, and obstacles within the line of sight that affect data resolution this investigation shows the utility of TLS for monitoring steep hillslopes in unstable glacial sediments.

References

Abellan, A., Calvet, J., Vilaplana, J.M., and Blanchard, J., 2010, Detection and spatial prediction of rockfalls by means of terrestrial laser scanner monitoring: Geomorphology, v. 119, no. 3-4, p. 162-171.

American Society for Testing and Materials, 2009, Standard Practice for Classification of Soils for Engineering Purposes (Unified Soil Classification System): ASTM D2487-11, ASTM International, West Conshohocken, PA www.astm.org.

American Society for Testing and Materials, 2009, Standard Practice for Description and Identification of Soils (Visual-Manual Procedure): ASTM D2488-09a, ASTM International, West Conshohocken, PA www.astm.org.

Anchor QEA, LLC, 2012, Final Alternatives Evaluation Report Gold Basin Landslide Study, *Prepared for Stillaguamish Tribe of Indians*, 167p.

Bellian, J.A., Kerans, C., and Jennette, D.C., 2005, Digital outcrop models: applications of terrestrial scanning lidar technology in stratigraphic modeling: Journal of Sedimentary Research, v. 7, no. 2, p. 166-176.

Benda, L., and Collins, B., 1992, Slope Stability Investigation of the Crown Pacific Property in the South Fork of the Stillaguamish River Basin, unpublished report, 37p.

Boehler, W., Bordas, V. M., and Marbs, A., 2003, Investigating laser scanner accuracy: Presented at the XIXth CIPA Symposium at Antalya, Turkey, Sept30-Oct4, 2003, 9p.

Booth, D.B. 1986, Formation of ice-marginal embankments into ice-dammed lakes in eastern Puget Lowland, Boreas, v. 15, p. 247-263.

Booth, D.B., 1989, Surficial Geologic Map of the Granite Falls 15-minute Quadrangle, Snohomish County, Washington: U.S. Geological Survey, scale 1:50,000, 3 sheets.

Buckley, S.J., Howell, J.A., Enge H.D., and Kurz, T.H., 2008, Terrestrial laser scanning in geology: data acquisition, processing and accuracy cosiderations: Journal of Geological Society, London, v. 165, p. 625-638.

Collins, B.D., Kayen, R., Reiss, T., and Sitar, N., 2007, Terrestrial LIDAR investigation of the December 2003 and January 2007 activations of the Northridge Bluff landslide, Daly City, California: U.S. Geological Survey open-file report 2007-1079, Version 1.0. ed., Reston, Va.: U.S. Geological Survey.

Cedarholm, C. J., and Salo, E. O., 1979, The Effects of Logging Road Landslide Siltation on the Salmon and Trout Spawning Gravels of Stequaleho Creek and the Clearwater

River Basin, Jefferson County, Washington 1972-1978, Open-File Report FRI-UW-7915, Fisheries Reseach Institute: University of Washington, 108p.

Chapman, D.W., 1988, Critical review of variables used to define effects of fines in redds of large salmonids. Trans. Am. Fish. Soc. 117: p.1-21.

Drury, T., 2001, Gold Basin Landslide Remediation Feasibility Study, Alternatives development and analysis, and preliminary project designs, RM 48, SF Stillaguamish River, *Prepared for the Stillaguamish Tribe of Indians*, 45p.

Dunning, S.A., Massey, C.I., and Rosser, N.J., 2009, Structural and geomorphological features of landslides in the Bhutan Himalaya derived from Terrestrial Laser Scanning: Geomorphology, v. 103 no. 1, 17p.

Greig, S. M., Sear D.A., and Carling, P.A., 2005, The impact of fine sediment accumulation on the survival of incubating salmon progeny: implications for sediment management, Science of the Total Environment, v. 344, no. 1-3, p. 241–258.

Ghuffar, S., Szekely, B., Roncat, A., and Pfeifer, N., 2013, Landslide Displacement Monitoring Using 3D Range Flow on Airborne and Terrestrial LiDAR Data: Remote Sensing, v. 5, p. 2720-2745.

Harpold, A. A., Marshall, J. A., Lyon, S. W., Barnhart, T. B., Fisher, B. A., Donovan, M., Brubaker, K. M., Crosby, C. J., Glenn, N. F., Glennie, C. L., Kirchner, P. B., Lam, N., Mankoff, K. D., McCreight, J. L., Molotch, N. P., Musselman, K. N., Pelletier, J., Russo, T., Sangireddy, H., Sjoberg, Y., Swetnam, T., and West, N., 2015, Laser vision: lidar as a transformative tool to advance critical zone science: Hydrology and Earth System Sciences, v. 19, p. 2881-2897.

Jaboyedoff, M., Oppikofer, T., Abellán, A., Derron, M., Loye, A., Metzger, R., and Pedrazzini, A., 2012, Use of LIDAR in landslide investigations: A review. *Natural Hazards,* v. 61, no. 1, p. 5-28.

Jusoff, Kamaruzaman, 2008, Estimating Acacia mangium Plantation's Standing Timber Volume Using an Airborne Hyperspectral Imaging System: The Open Forest Science Journal, v. 7, no. 1, p.61-67

Jusuf, S. K., Wong, N. H., Hagen, E., Anggoro, R., and Hong, T., 2007, The influence of land use on the urban heat island in Singapore: Habitat International, v. 31, no. 2, p.232-242

Katz, O., and Mushkin, A., 2013, Characteristics of sea-cliff erosion induced by a strong winter storm in the eastern Mediterranean: Quaternary Research, v. 80, p.20-32.

Keaton, J. R., Wartman, J., Anderson, S., Benoit, J., deLaChapelle, J., Gilbert, R., Montgomery, D. R., 2014, The 22 March 2014 Oso Landslide, Snohomish County, Washington: Geotechnical Extreme Events Reconnaissance *Turning Disaster into Knowledge*, Sponsored by the National Science Foundation, 186p.

Koloski, J. W., Schwarz, S. D., and Tubbs, D. W., 1989, Geotechnical properties of geologic materials: Engineering Geology, *in* Washington, Richard W. Galster, ed., Washington Division of Geology and Earth Resources Bulletin 78, v. I, p. 19-26.

Lato, M., Hutchinson, J., Diederichs, D., Harrap, R., and Ball, D., 2009, Engineering monitoring of rockfall hazards along transportation corridors: Using mobile terrestrial LiDAR, Natural Hazards and Earth System Science, v. 9, no. 3, p. 935-946.

Lewis, J., 1996, Turbidity-controlled suspended sediment sampling for runoff-event load Estimation, Water Resources. Res., v.32, p.2299-2310.

Lloyd, D.S., 1987, Turbidity as a water quality standard for salmonid habitats in Alaska, North American Journal Fish Management, v.7, p.34-45.

Miller, D., 1999, Hazel/Gold Basin Landslides: Geomorphic Review Draft Report, M2 Environmental Services, 16p.

Mikhail, G. N., and Rachold, V., 1999, Computer Techniques for Measurement of Coastal Retreat in the Russian Arctic: Geological Survey of Canada, open-file report 3929, p.10

Minder, J.R., Roe, G.H., and Montgomery, D.R., 2009, Spatial patterns of rainfall and shallow landslide susceptibility: Water Resources Research, v. 45, 11p.

Mushkin, Amit, 2015, ESS 590D Labs and Manual, ESS 590D: Applied LiDAR research, Earth and Space Science Department, University of Washington.

National Marine Fisheries Service (NMFS), 1996, Coastal salmon conservation: working guidance for comprehensive salmon restoration initiatives on the Pacific Coast, USDC-NOAA, NMFS, Portland, OR

Petrie, G., and Toth, C. K., 2008, Introduction to Laser Ranging, Profiling, and Scanning: Topographic Laser Ranging and Scanning: Priniciples and Processing, 28p.

Pollock, M. M., Beechie, T. J., Liermann, M., and Bigley, R. E., 2009, Stream Temperature Relationships to Forest Harvest in Western Washington: JAWRA Journal of the American Water Resources Association, v. 45, p.141–156.

Purser, M. D., Gaddis, B., and Rhodes, J. J., 2009, Primary Sources of Fine Sediment *In the South Fork Stillaguamish River*: Snohomish County Public Works *Surface Water Management* (Recreation and Conseravation Office Project 05-1564N), 89p.

Rengers, F. K., and Tucker, G. E., 2015, The evolution of gully headcut morphology: a case study using terrestrial laser scanning and hydrological monitoring: Earth Surface Processes and Landforms, v. 40, no. 10, p.1304-1317.

Rengers, F. K., Tucker, G. E., Moody, J. A., and Ebel, B.A., 2016, Illuminating Wildfire Erosion and Deposition Patterns with Repeat Terrestrial Lidar: Journal of Geophysical Research: Earth Surface, v. 121, 58p.

Rhodes, J. J., Greene, M. J., Purser, M.D., 2001, Annual Project Report for 2000: Monitoring Fine Sediment in Salmon Habitat in John Day and Grande Ronde Rivers. BPA Report DOE/BP-00004272-1, BPA, Portland, OR.

Rhodes, J. J., McCullough, D. A., and Espinosa Jr., F. A., 1994, A coarse Screeening Process for Evaluation of the Effects on Land Management Activities on Salmon Spawning and Rearing Habitat in ESA Consultations: CRITFC Technical Report 94-4

Rhodes, J. J., and Purser, M. D., 1998, Overwinter Sedimentation of Clean Gravels in Simulated Redds in the Upper Grande Ronde River and Nearby Streams in Northeastern Oregon, USA: Implications for the Survival of Threatened Spring Chinook Salmon. Pages 403-412 *in* M.K. Brewin and D.M.A. Monita, tech. Coords. Forest-fish conference: land management practices affecting aquatic ecosystems. Proc. Forest-Fish Conf., May 1-4, 1996, Calgary, Alberta. Nat. Resour. Can., Can. For., Serv., North For. Cent., Edmonton, Alberta. Inf. Rep NOR-X-356.

Riegl, 2015, Riegl VZ-4000: Terrestrial Laser Scanning, Riegal Laser Measurement Systems, 6p.

Rohrbaugh, N. B., 2015, A new technique for modeling the geomorphology of a slow moving, soft-slope landslide using terrestrial LiDAR (M.S. thesis): Missouri University of Science and Technology, 72p.

Savage, W. Z., Morrissey, M. M., and Baum, R.L., 2000, Geotechnical Properties for Lanslide-Prone Seattle – Area Glacial Deposits, United States Geological Survey Open-File Report 00-228, 6p.

Seattle Times, The, 2014, Landslide risk keeps popular campground closed, Local News, The Seattle Times, July 12, 2015.

Shannon & Wilson Engineers, 1954, Report on slide on South Fork Stillaguamish River at Gold Basin Forest Camp, to the State of Washington Departments of Fisheries, 14p. Plus appendix, 9 plates.

Shaw, J., Gilbert, R., and John ,J. J. Archer, 1978, Proglacial Lacustrine Sedimentation during Winter: Arctic and Alpine Research, v. 10, no. 4, p. 689–699.

Shilpakar, P., Oldow, J. S., Walker, J. D., and Whipple, K. X., 2016, Assessment of the uncertainty budget and image resolution of terrestrial laser scans of geomorphic surfaces: Geosphere, v. 12, no. 1, 25p.

Shipman, H., 2001, Coastal Landsliding on Puget Sound: A review of landslides occurring between 1996 and 1999: Washington State Department of Ecology Open-File Report 01-06-019, 101p.

Sigler, J.W., Bjornn, T.C., and Everest, F.H., 1984, Effects of Chronic Turbidity on Density and Growth of Steelheads and Coho Salmon: Transactions of the American Fisheries Society v.113, p.142-150.

Tabor, R.W., Booth, D.B., Vance, J.A., and Ford, A.B., 1988, Geologic Map of the Sauk River 30-by 60-minute Quadrangle, Washington: United States Geological Survey Open-File Report 88-692.

Tabor, R.W., Booth, D.B., Vance, J.A., and Ford, A.B., 2002, Geologic map of the 30- by 60-minute Quadrangle, Washington: U.S. Geological Survey, scale 1:100,000, 3 sheets.

Tubbs, D., 1974, Landslides in Seattle, Division of Geology and Earth Resources Information Circular 52, Department of Natural Resources, Olympia, Washington.

Western Regional Climate Center, 2016, Recent climate in the west, Darrington Ranger Station, Darrington, WA, Accessed February 21, 2016, www.wrcc.dri.edu

Figure 1 – Location map showing the location of the Gold Basin Landslide Complex (GBLC) and the site of the 2014 Oso, WA Landslide. The GBLC resides on the north bank of the South Fork of the Stillaguamish River. The site of the 2014 Oso, WA Landslide resides on the north bank of the North Fork of the Stillaguamish River.

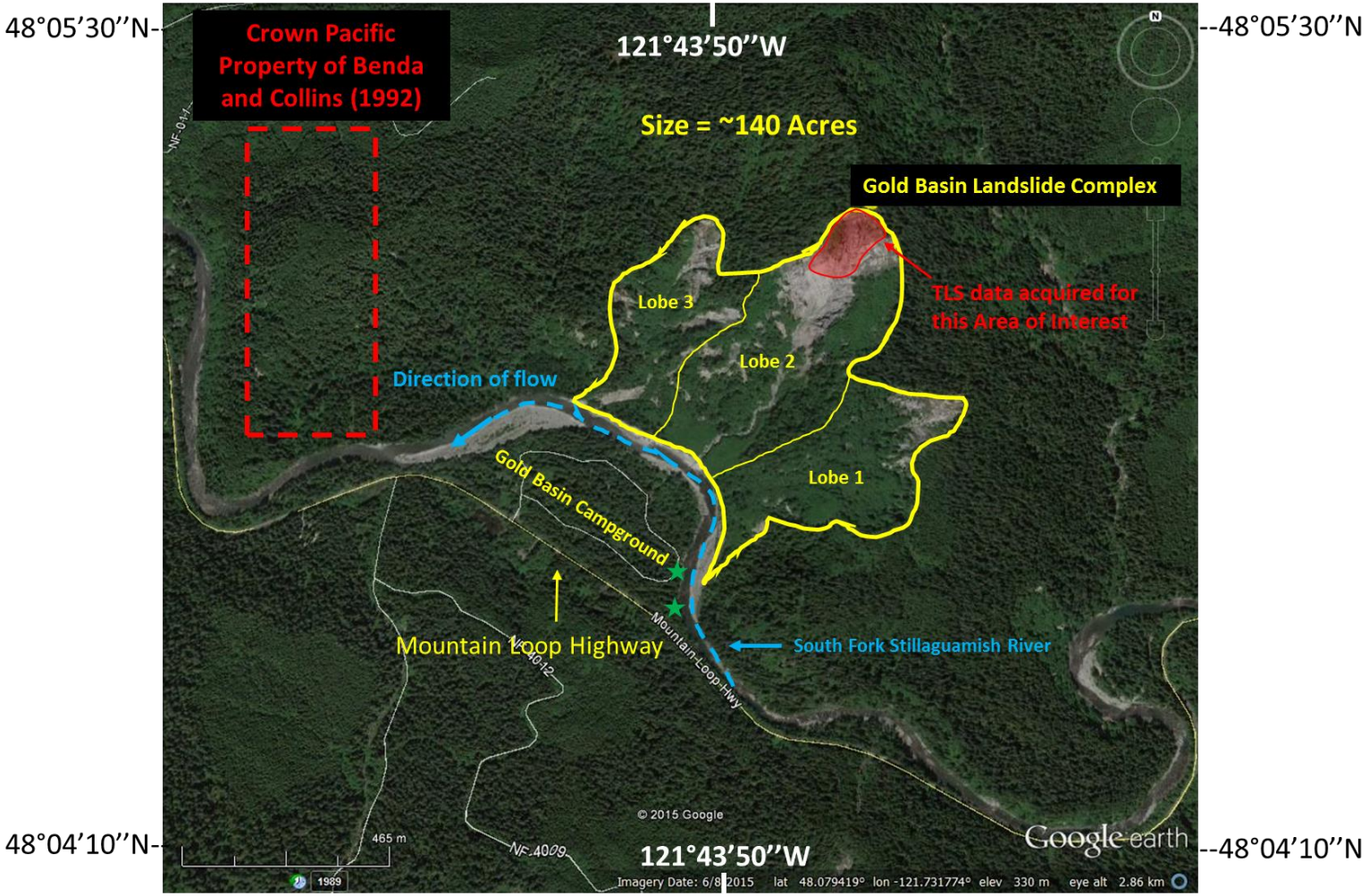

Figure 2 –The Gold Basin Landslide Complex (GBLC) and its relation to the South Fork Stillaguamish River. The Crown Pacific Property was the site area of the Benda and Collins (1992) study. The two scan locations used for this study are marked by the green stars on the south bank east of the Gold Basin Campground. The area of interest for this study is outlined by the red polygon to the north (Figures 6-9).

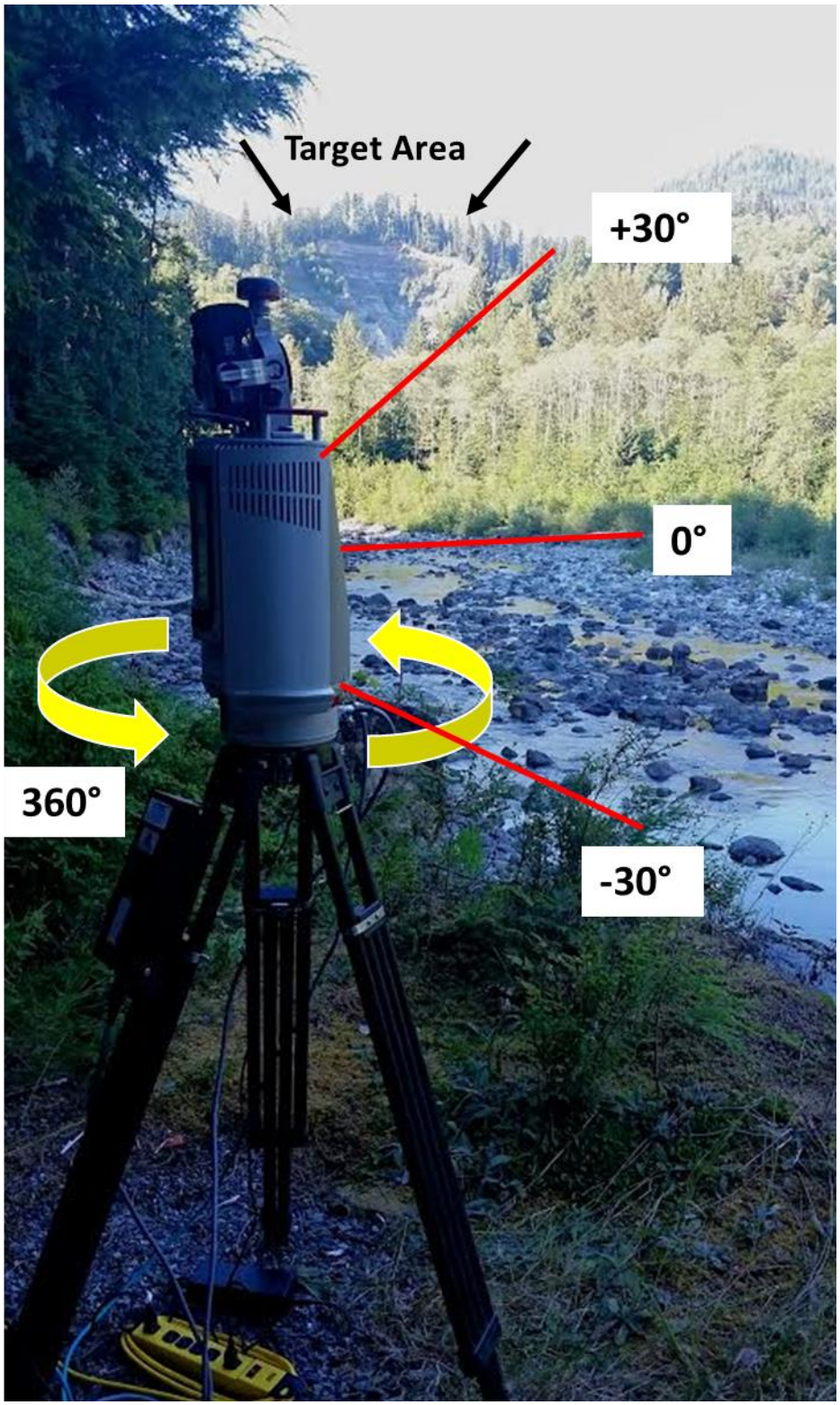

Figure 3 – Photo of the Reigl VZ-4000 Terrestrial LiDAR Scanner at scan position 1 on the east extent of the Gold Basin Campground. Note the range in which the VZ 4000 has the ability to scan. The tripod and scanner are approximately 1.8m tall. The target area in the background is ~1.1km away. Photo is facing north.

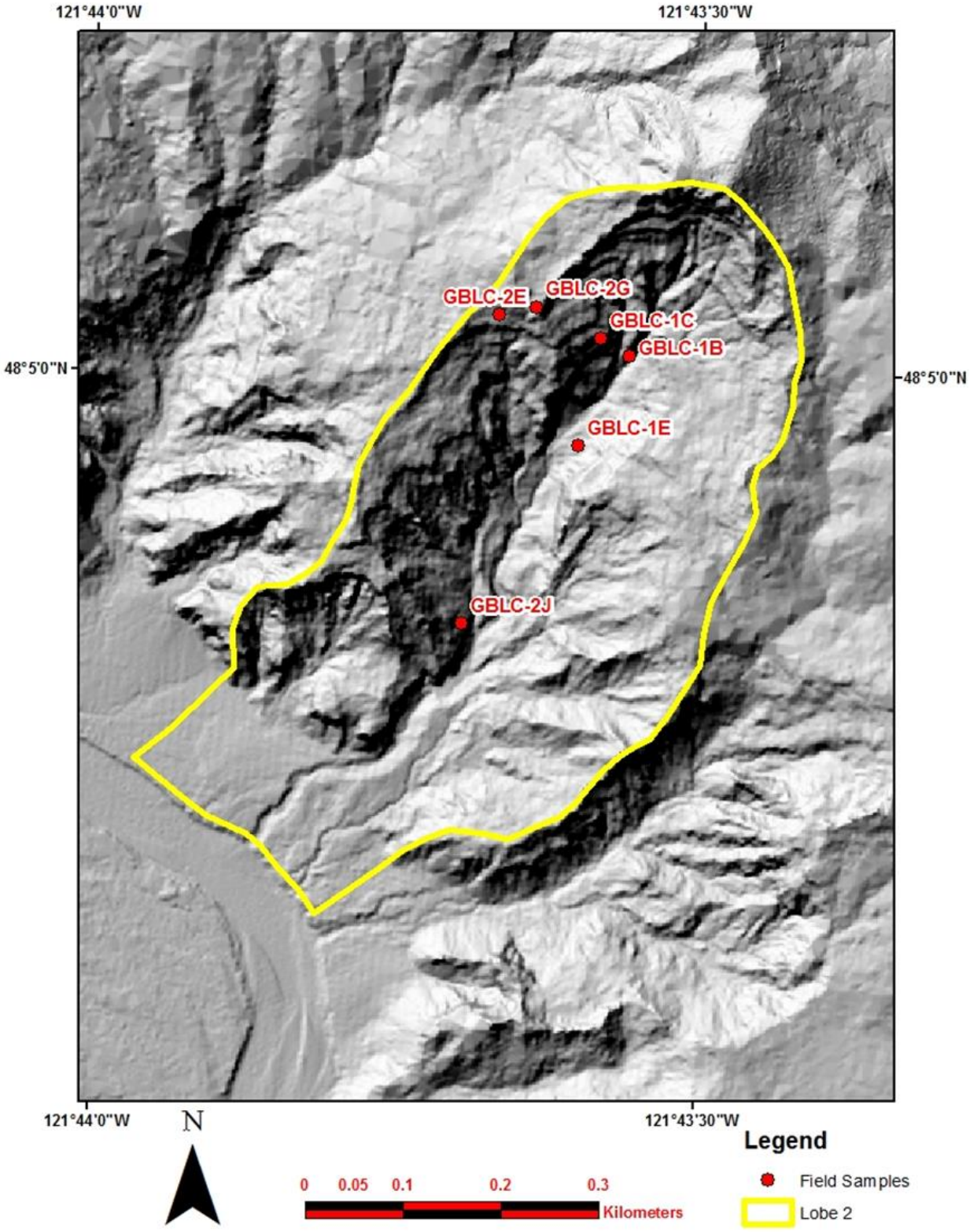

Figure 4 – LiDAR hillshade map showing sample locations used for the creation of the generalized stratigraphic column. Lobe 2 is outlined in the yellow polygon. (LiDAR data 6ft/pixel (1.8m/pixel) was taken from www.pugetsoundlidar.ess.washington.edu).

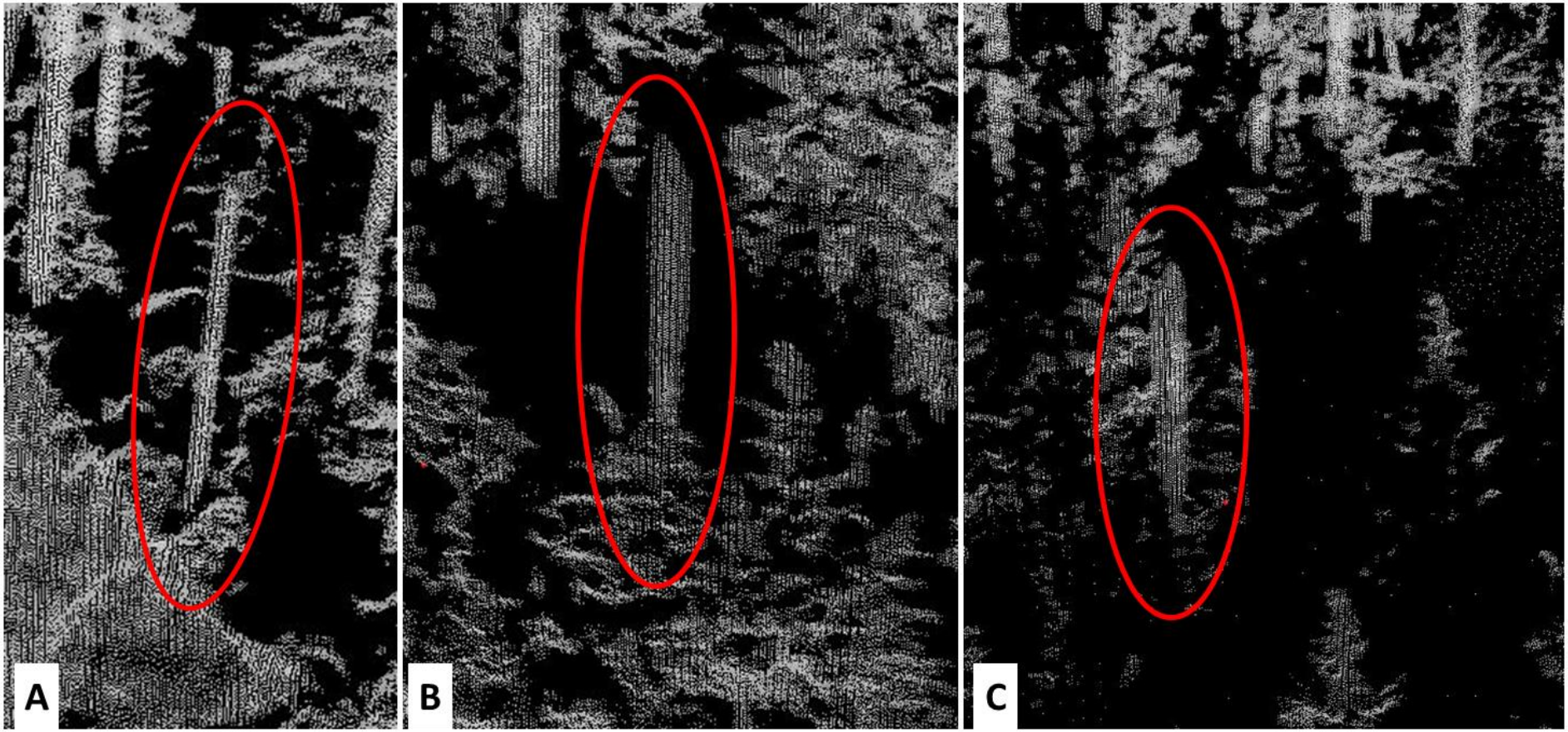

Figure 5 – Examples of the tree stumps used for registering scan positions together. Images were obtained from the epoch3 data set. When performing co-registration, it is important that the same part of the tree is used every time (i.e. very top, very bottom, large branch). Marked stumps in A, B, and C are 0.5m, 1.0m, and 0.7m across, respectively.

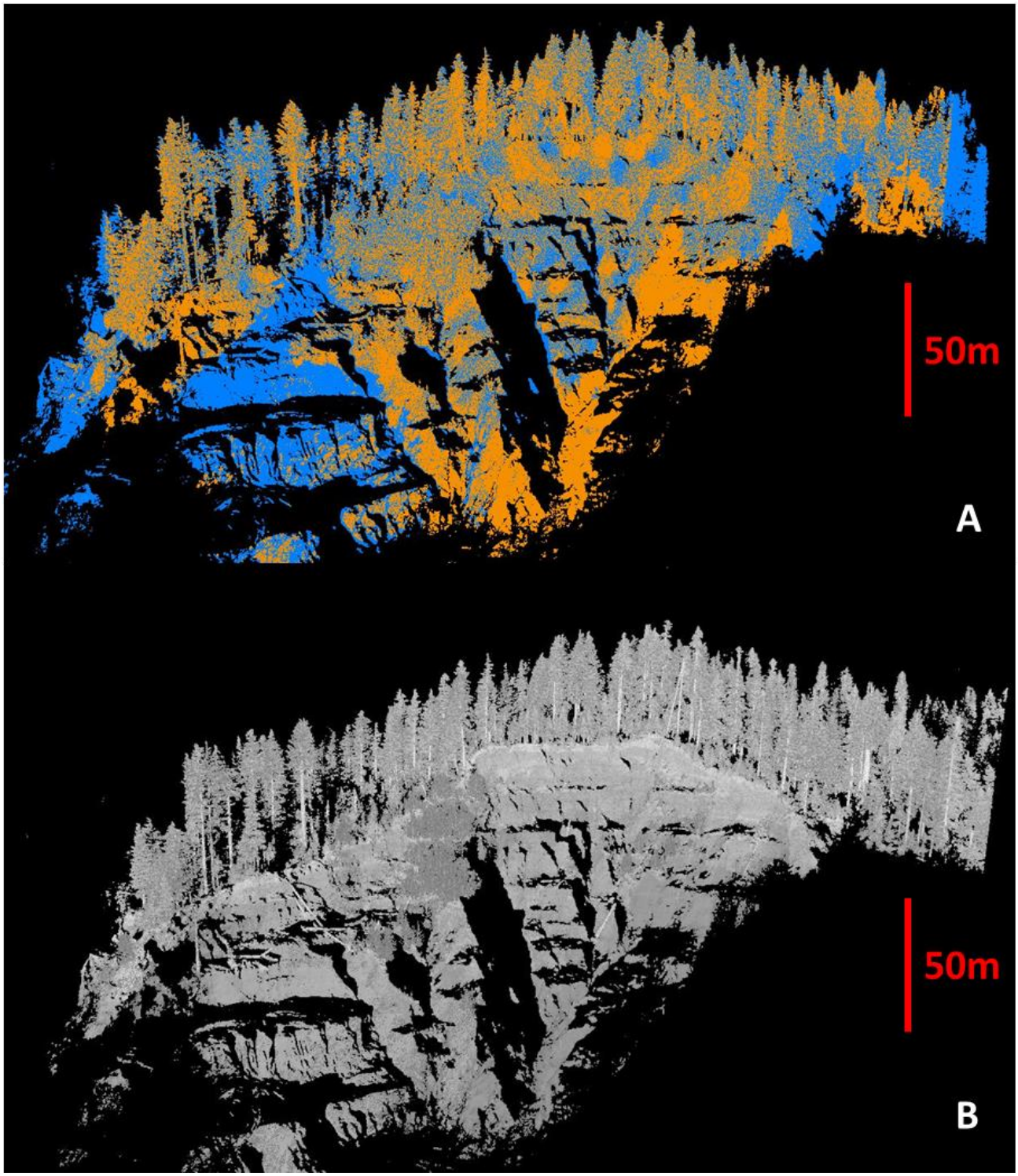

Figure 6 – 3D point clouds obtained from epoch3 scan. A shows data from scan position 1 in orange and data from scan position 2 in blue. B shows the combined scans in a grey scale. Black represents no data areas due to occlusions. Both point clouds are facing north. See Figure 2 for location.

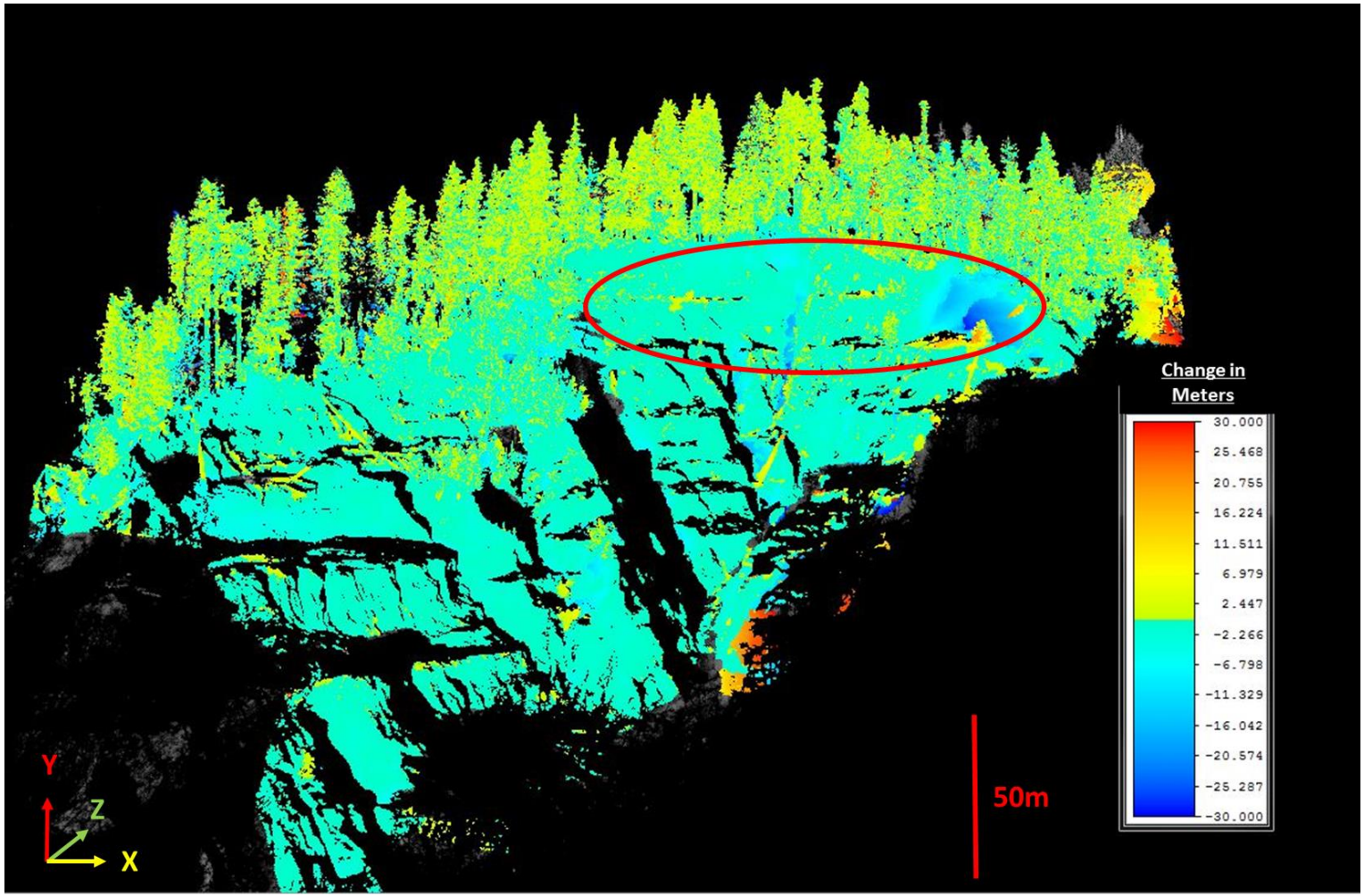

Figure 7 – Suface comparison between epoch2 and epoch3 along the vertical, cliff-normal plane. The area of interest (northeast headwall) is located within the red circle. View is facing north similar to that of the images in Figure 6. Note the addition of the tree stump in the upper right corner. See Figure 2 for location.

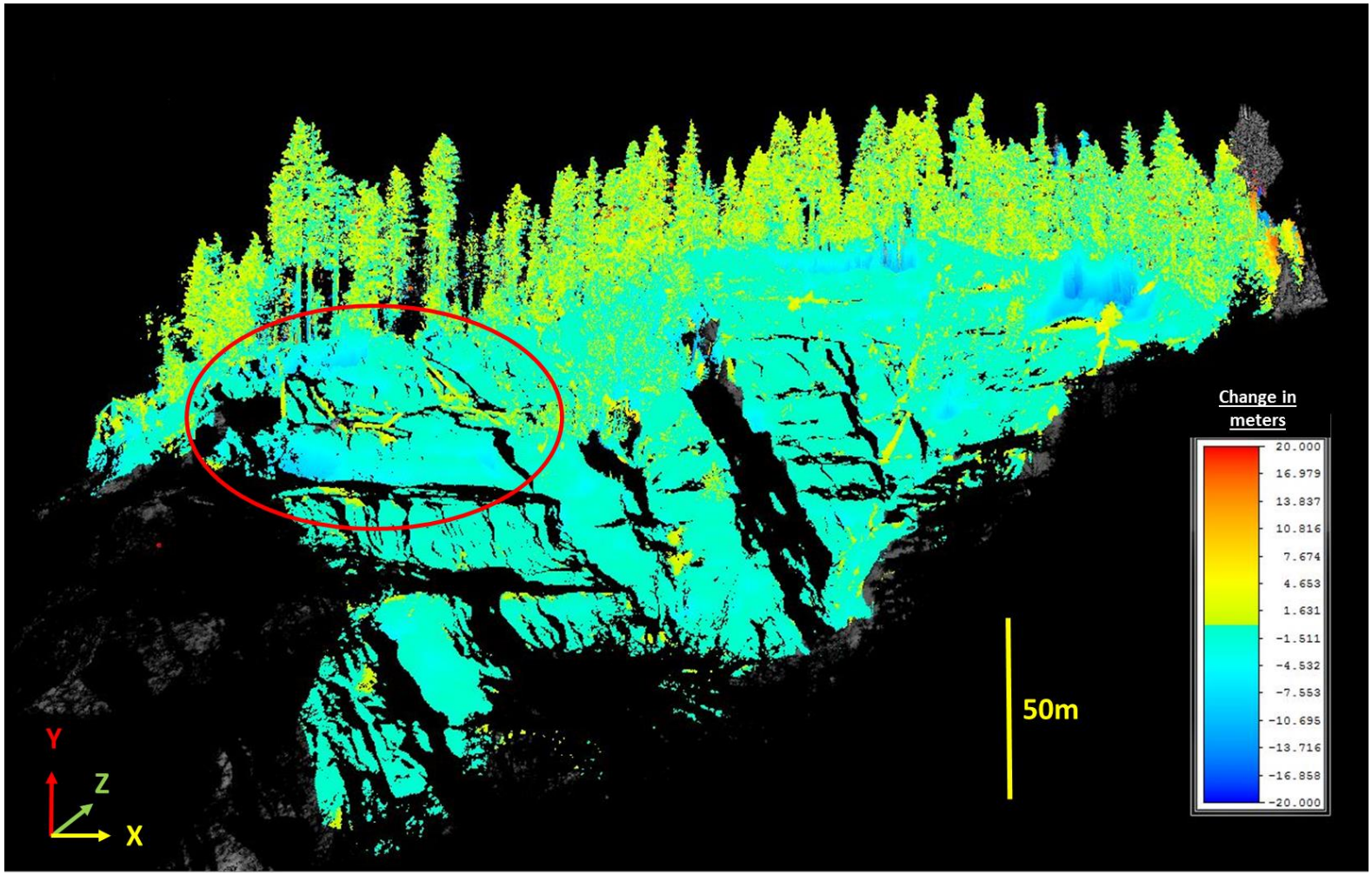

Figure 8 – Surface comparison between epoch2 and epoch3 along the vertical, cliff-normal plane. Note that the northeast corner was not the only area to experience erosion, note the blue shades circled in red on the left side of the image. Black represents no data areas due to occlusions. Image is facing north. See Figure 2 for location.

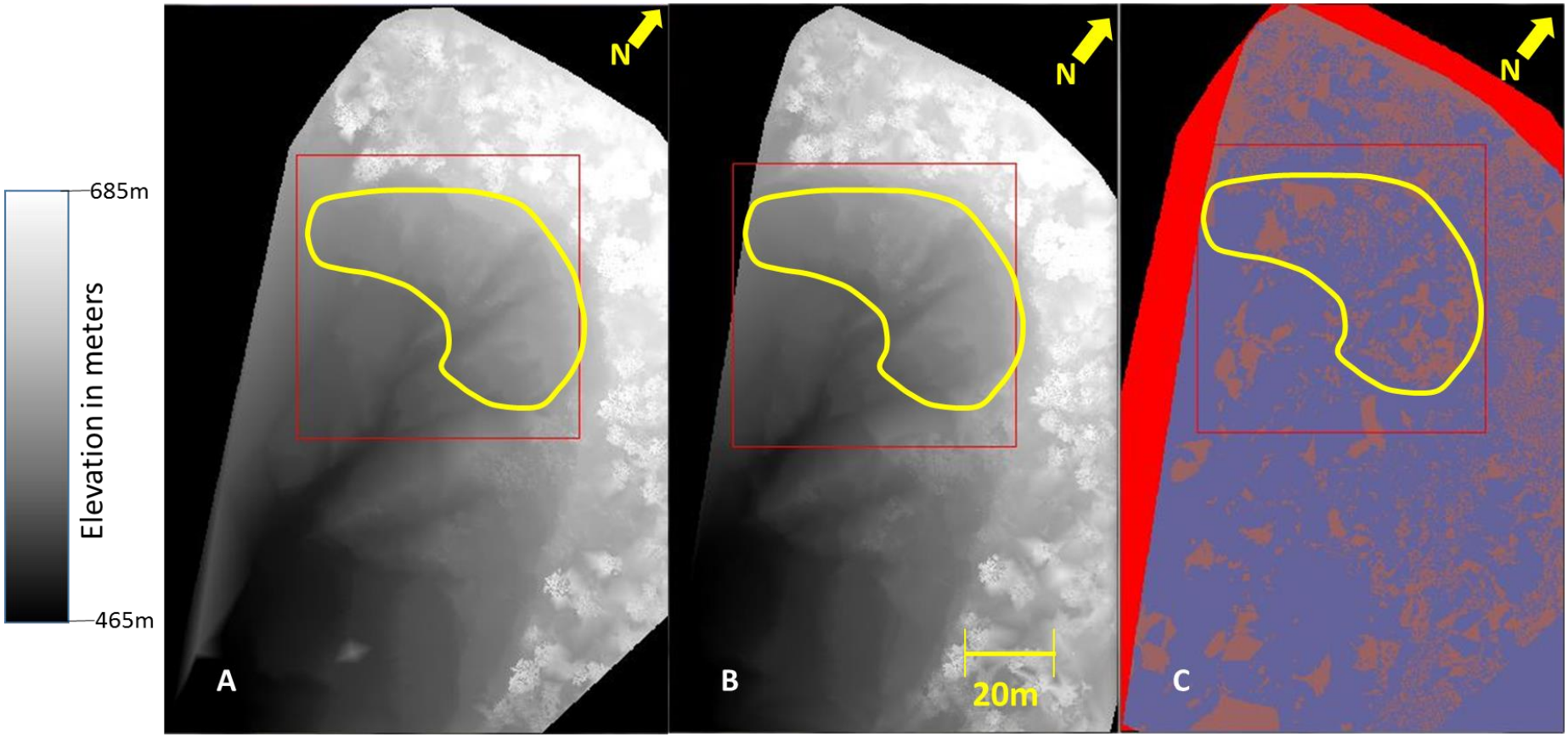

Figure 9 – Comparison of DEMs from epoch3 (A, January 2016) and epoch2 (B, September 2015). The area of interest is outlined by the yellow polygon in the three images. C shows the change detected after post-processed in ENVI. Blue is where no changes occurred and orange represents areas where measureable erosion between epoch2 and epoch3 occurred. The total area in all of these images is ~25,600m^2. See Figure 2 for location.

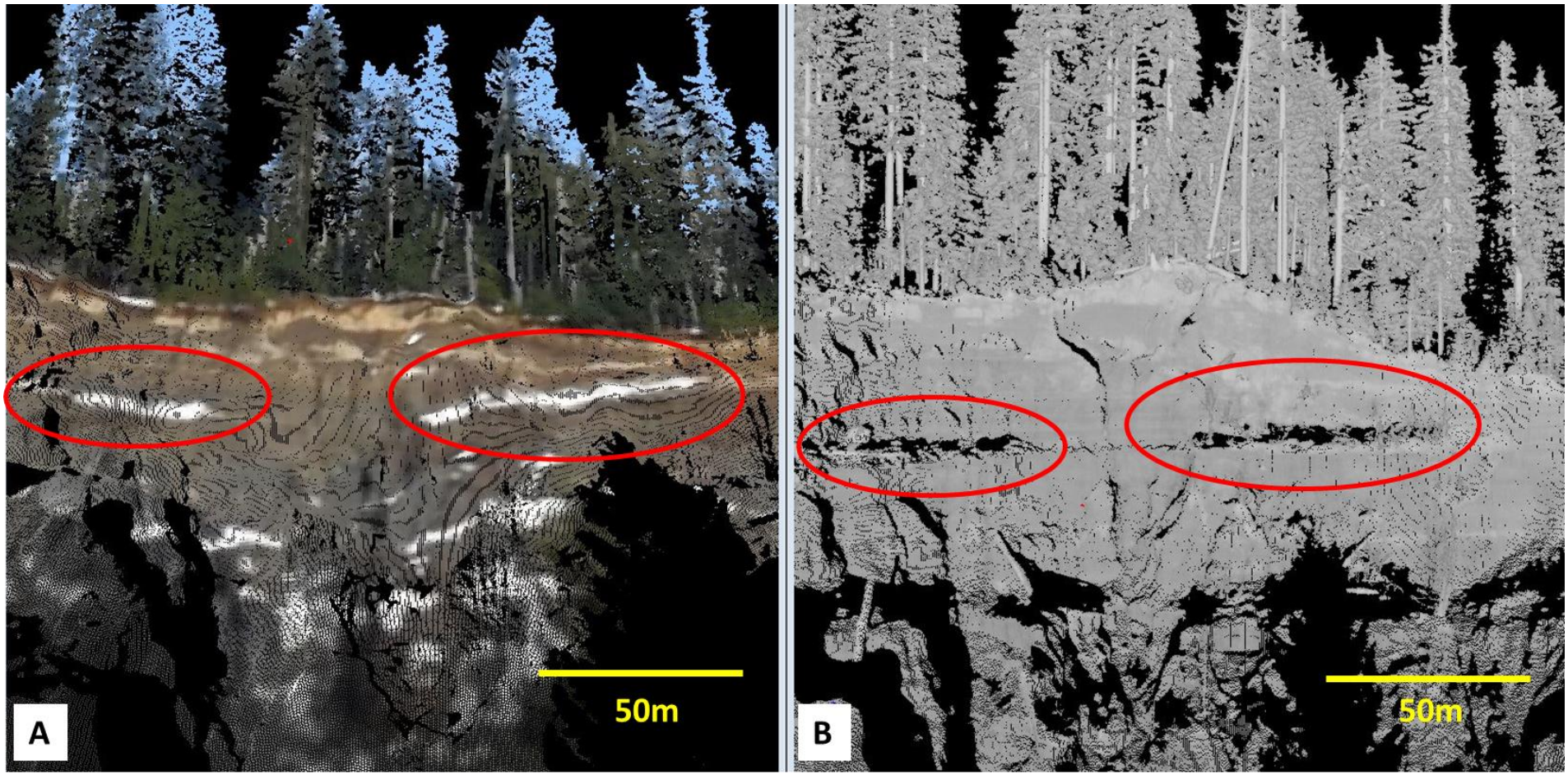

Figure 10 – Comparison of 3D point cloud data with digital photo mosaic (A) and a grayscale image (B) facing northeast within Lobe 2 of the GBLC. Note the areas circled in red showing where data gaps occurred due to snow.

Figure 11 – Photo of a debris flow deposit along the right bank of the South Fork of the Stillaguamish River. The materials surrounding the large log is a chaotic deposit that consists of gravels, sands, silts, and clays. The vegetation overlying this deposit is mostly juvenile alders. The log is. 0.5m in diameter.

Figure 12 – Photo of a clay/silt block failure along the eastern wall within Lobe 2 of the GBLC. During my field investigations I observed a large block of silts and clays fall from the wall above the red line, then land and crumble as it was deposited within the gully outlined by the yellow circle. The face of the cliff is ~50m tall. The photo is facing east along the eastern extent of Lobe 2 (Figure 2).

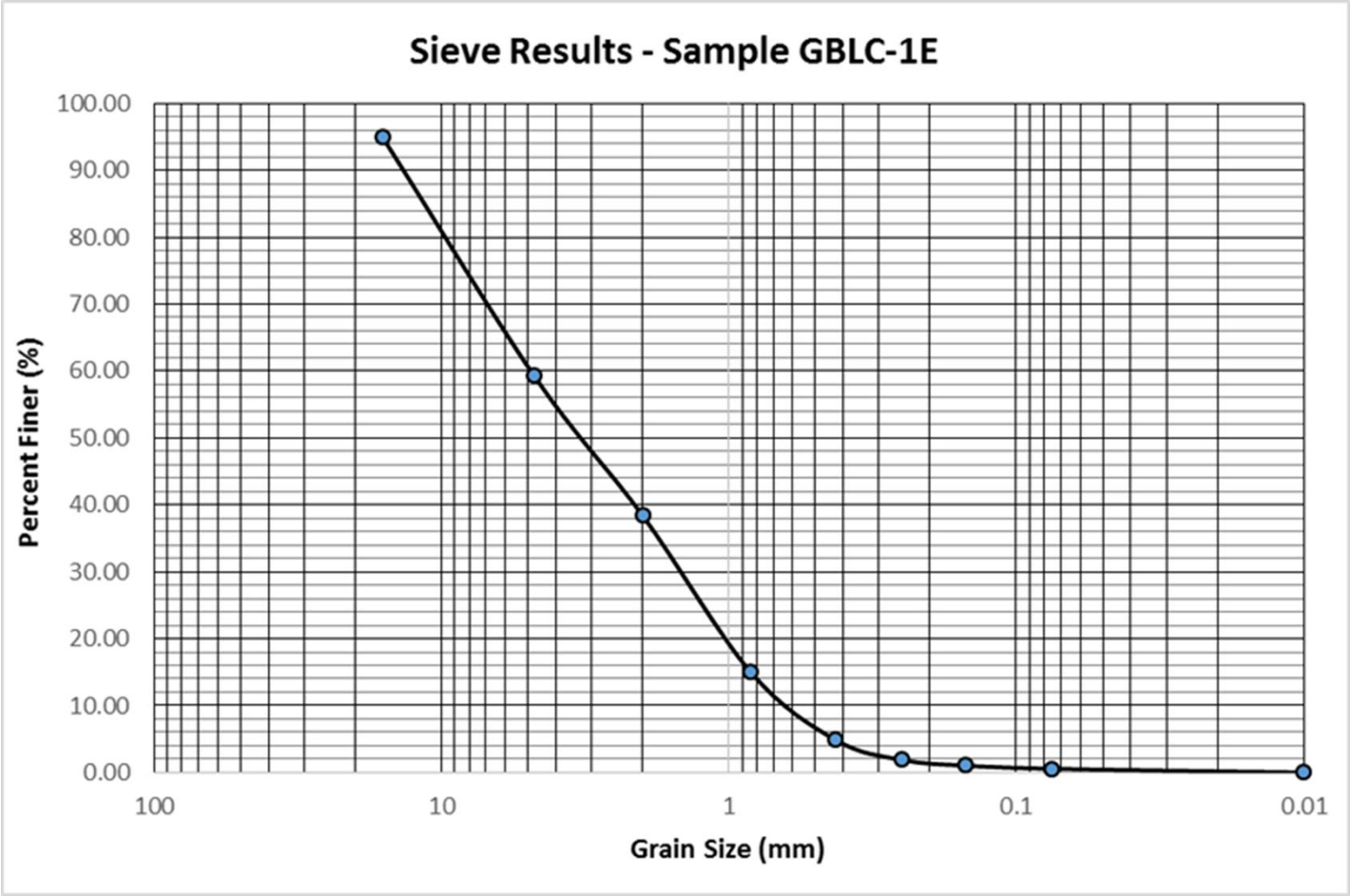

Figure 13 – Grain size distribution chart for coarse grain sample GBLC-1E. Classification results can be found in Table 1. Data can be found in Appendix A. Note that ~12% of grains are below 0.85mm which is the sediment size outlined by previous studies to be harmful to salmon embryos (e.g. Cederhold and Salo, 1979; Chapman, 1988; NMFS, 1996; Purser et al., 2009).

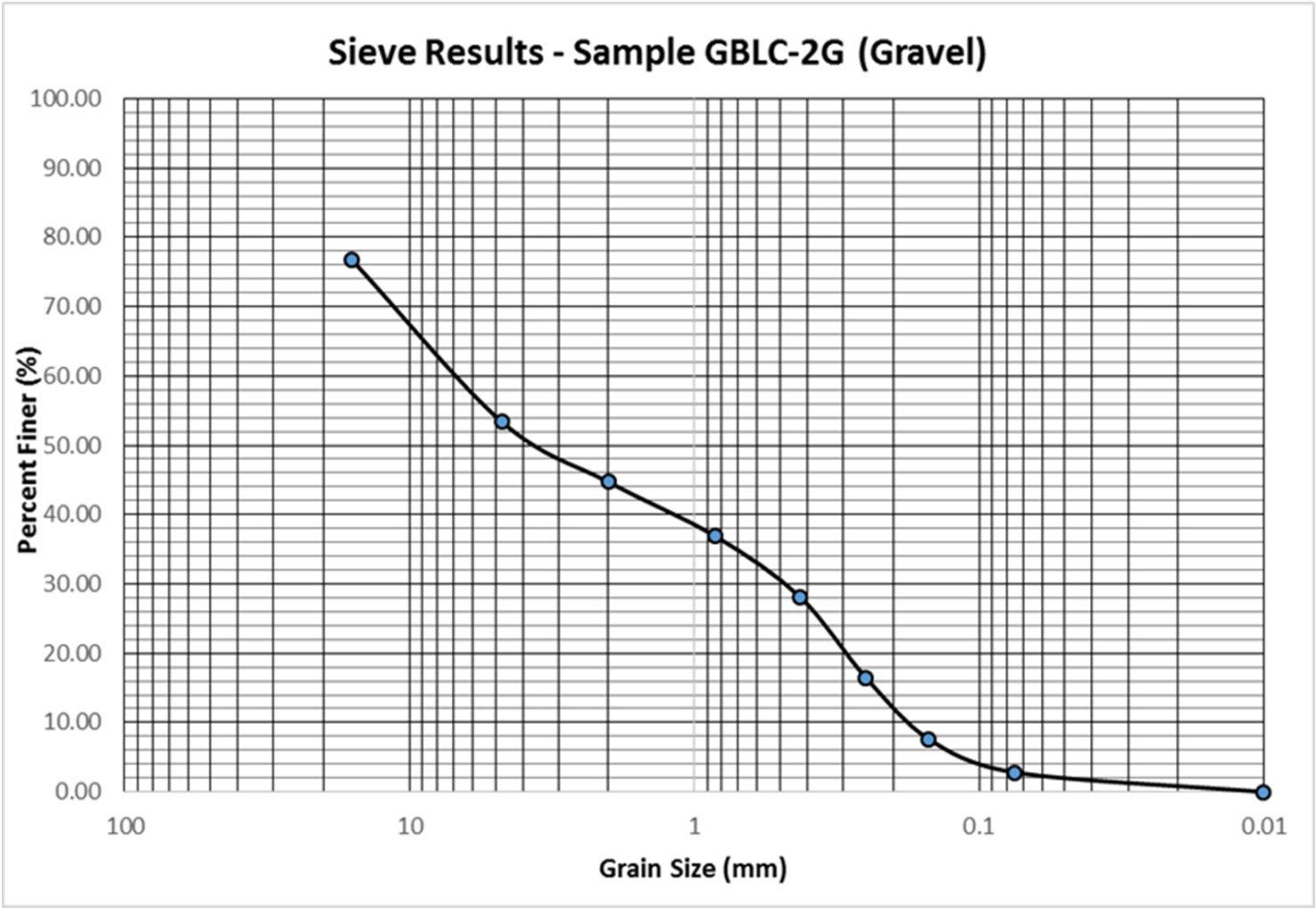

Figure 14 – Grain size distribution chart for coarse grain sample GBLC-2G (gravel). Classification results can be found in Table 1. Data can be found in Appendix A. Note that ~35% of grains are below 0.85mm which is the sediment size outlined by previous studies to be harmful to salmon embryos (e.g. Cederhold and Salo, 1979; Chapman, 1988; NMFS, 1996; Purser et al., 2009).

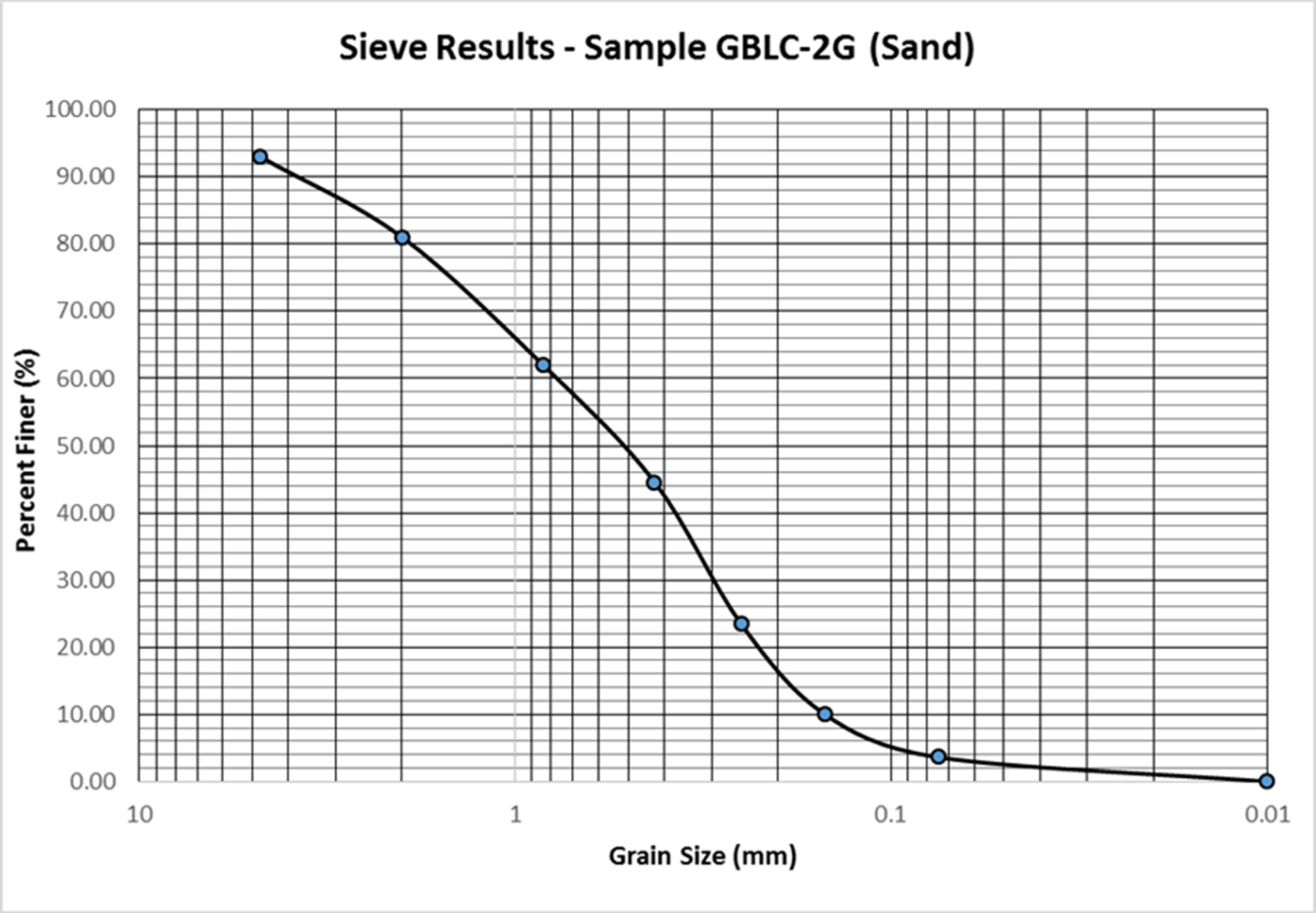

Figure 15 – Grain size distribution chart for coarse grain sample GBLC-2G (sand). Classification results can be found in Table 1. Data can be found in Appendix A. Note that ~58% of grains are below 0.85mm which is the sediment size outlined by previous studies to be harmful to salmon embryos (e.g. Cederhold and Salo, 1979; Chapman, 1988; NMFS, 1996; Purser et al., 2009).

Figure 16 – Grain size distribution chart for coarse grain sample GBLC-2J. Classification results can be found in Table 1. Data can be found in Appendix A. Note that ~80% of grains are below 0.85mm which is the sediment size outlined by previous studies to be harmful to salmon embryos (e.g. Cederhold and Salo, 1979; Chapman, 1988; NMFS, 1996; Purser et al., 2009).

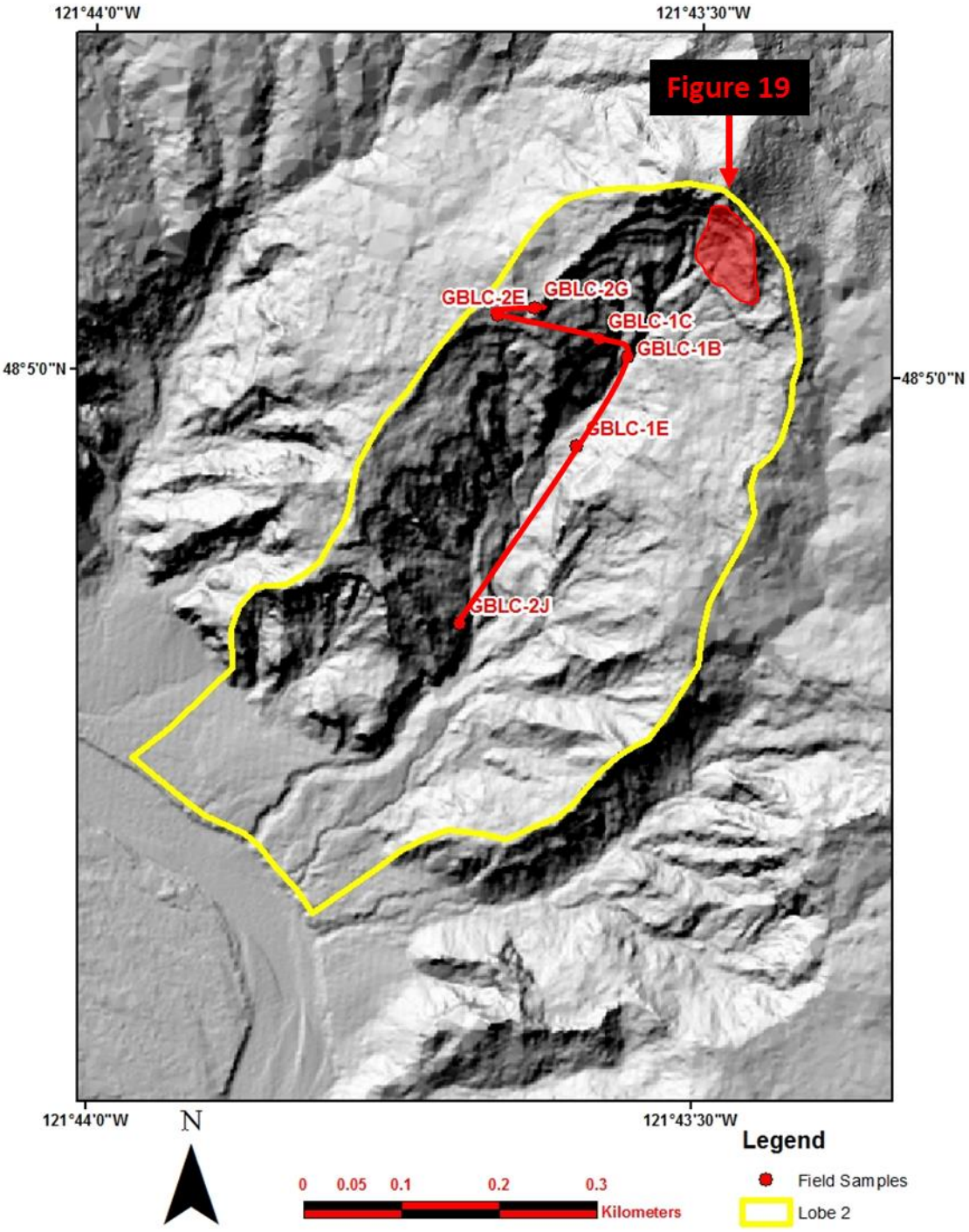

Figure 17 – LiDAR image of the study area and field sites where samples were collected. The generalized stratigraphic column in Figure 18 was created using the sites in order from lowest elevation to highest as outlined by the red line connecting the field sites. The red polygon represents the location of Figure 19. (LiDAR data 6ft/pixel (1.8m/pixel) was taken from www.pugetsoundlidar.ess.washington.edu).

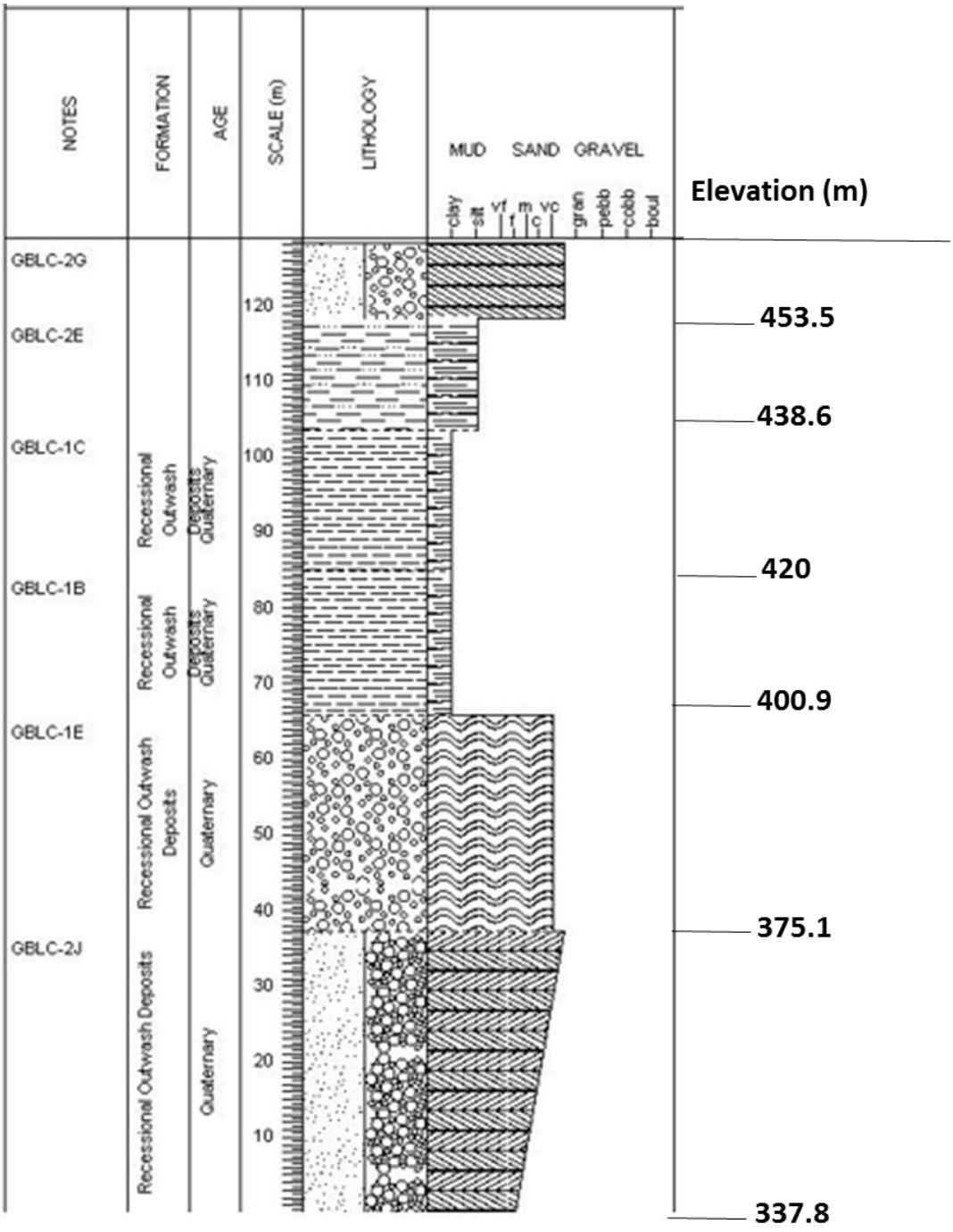

Figure 18 – Generalized stratigraphic column of Lobe 2 within the GBLC. This column was created from a compilation of field investigations and lab analyses (See Figure 17 and Table 1). Note the 50m section of silts and clays between strata of poorly sorted gravels and sands. This represents a thick section of impermeable materials, making it an avenue for perched groundwater.

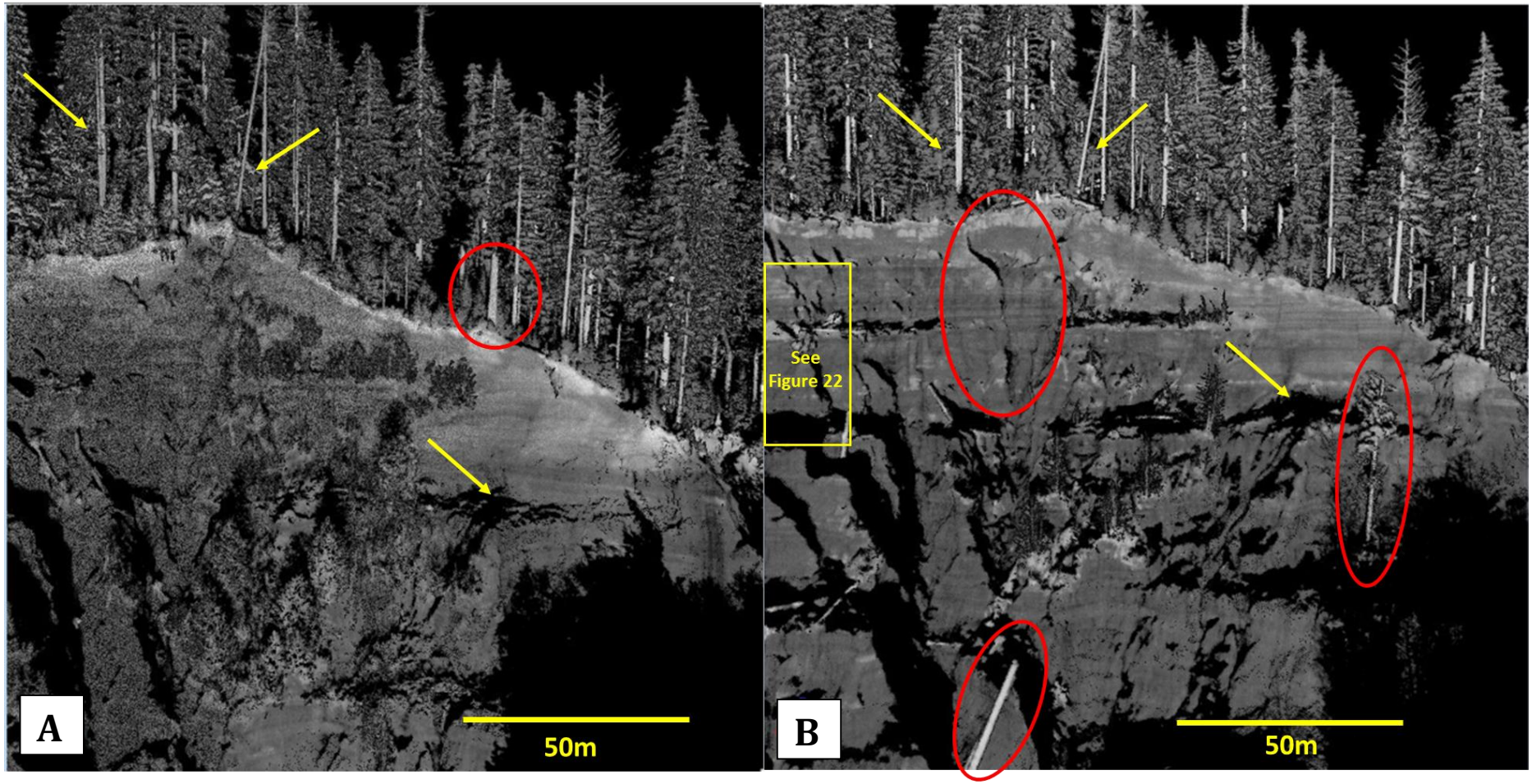

Figure 19 – Comparison of epoch1 (A) and epoch3 (B) point cloud data. Notice that some trees stumps from epoch1 (i.e. stump circled in red in A) are no longer present in epoch3. Also note the addition of a large tree in the lower corner of photo B (circled in red) and large erosional impression (also circled in red) Yellow arrows point to landforms and trees that can be used as "benchmarks" when comparing epochs. The yellow box in B represents location of Figure 22. Image is facing northeast. See Figure 17 for location.

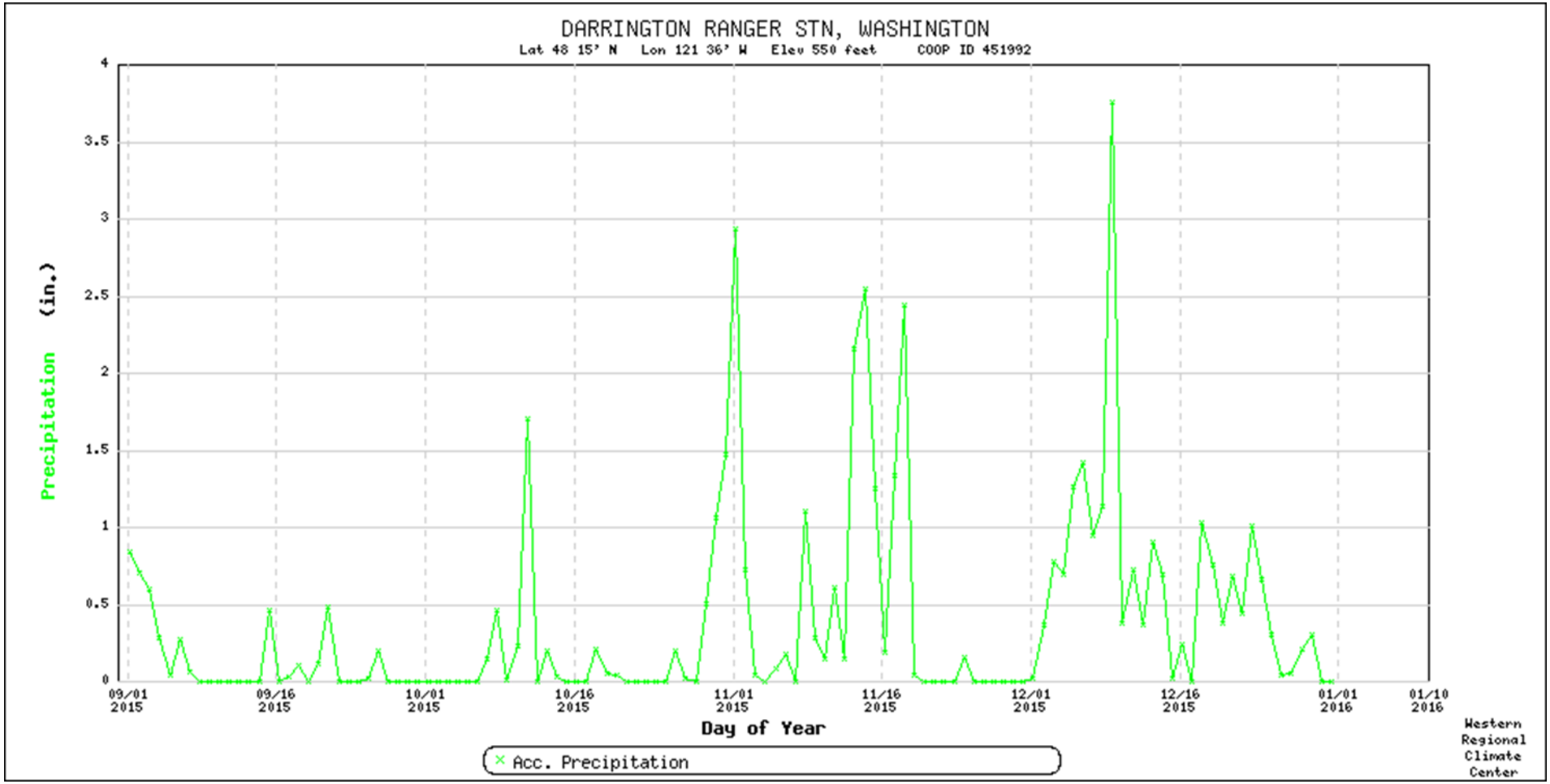

Figure 20 – Graph of precipitation data at Darrington Ranger Station (~20km north of study area). There was at least three times between epoch2 (September 19, 2015) and epoch3 (January 10, 2016) where rain exceeded 44.45mm (1.75in). According to Tubbs (1974) if rain exceeds 44.45mm (1.75in) in a twenty four period there is a 70% chance of landslide failure.

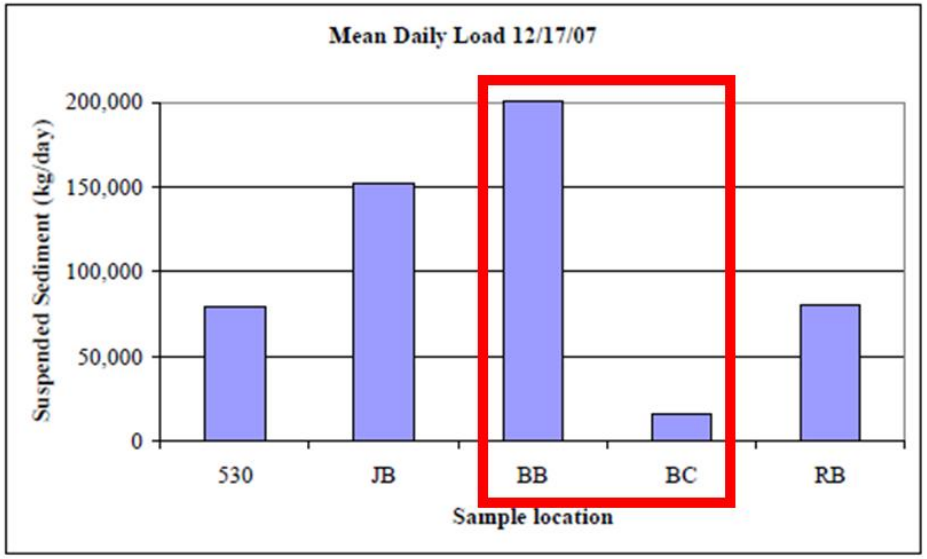

location	date sampled (yymmdd)	TSS (mg/L)
SFADC	071114	1
SFADC	071114	1
530	071205	11
530	071205	133
530	071205	19
JB	071205	156
JB	071205	152
JB	071205	168
RP	071205	64
RP	071205	61
RP	071205	61
CC	071205	29
CC	071205	30
[illegible]	[illegible]	[illegible]
BB	071205	51
BB	071205	79
BB	071205	37
BC	071205	217
BC	071205	176
BC	071205	176
[illegible]	[illegible]	[illegible]
RB	071205	95
RB	071205	110
DC	071205	98
DC	071205	89
DC	071205	97
SFADC	071205	26
SFADC	071205	27
SFADC	071205	25

Figure 21 – The bar graph on the left shows suspended sediment (kg/day) upstream (BC) and downstream (BB) of the GBLC on December 12, 2007. The table on the right shows total suspended solid (TSS) measurements collected upstream (BC) and downstream (BB) of the GBLC on December 5, 2007. The collection site "BC" is located ~7 km upstream of the GBLC, while the collection site 'BB" is located ~2km downstream of the GBLC (Purser et al., 2009) From the data collected between epoch2 (September 2015) and epoch3 (January 2016) I calculated a potential TSS of ~110mg/L and a suspended sediment load of ~80,000kg/day. Refer to section 7.2 for more information.

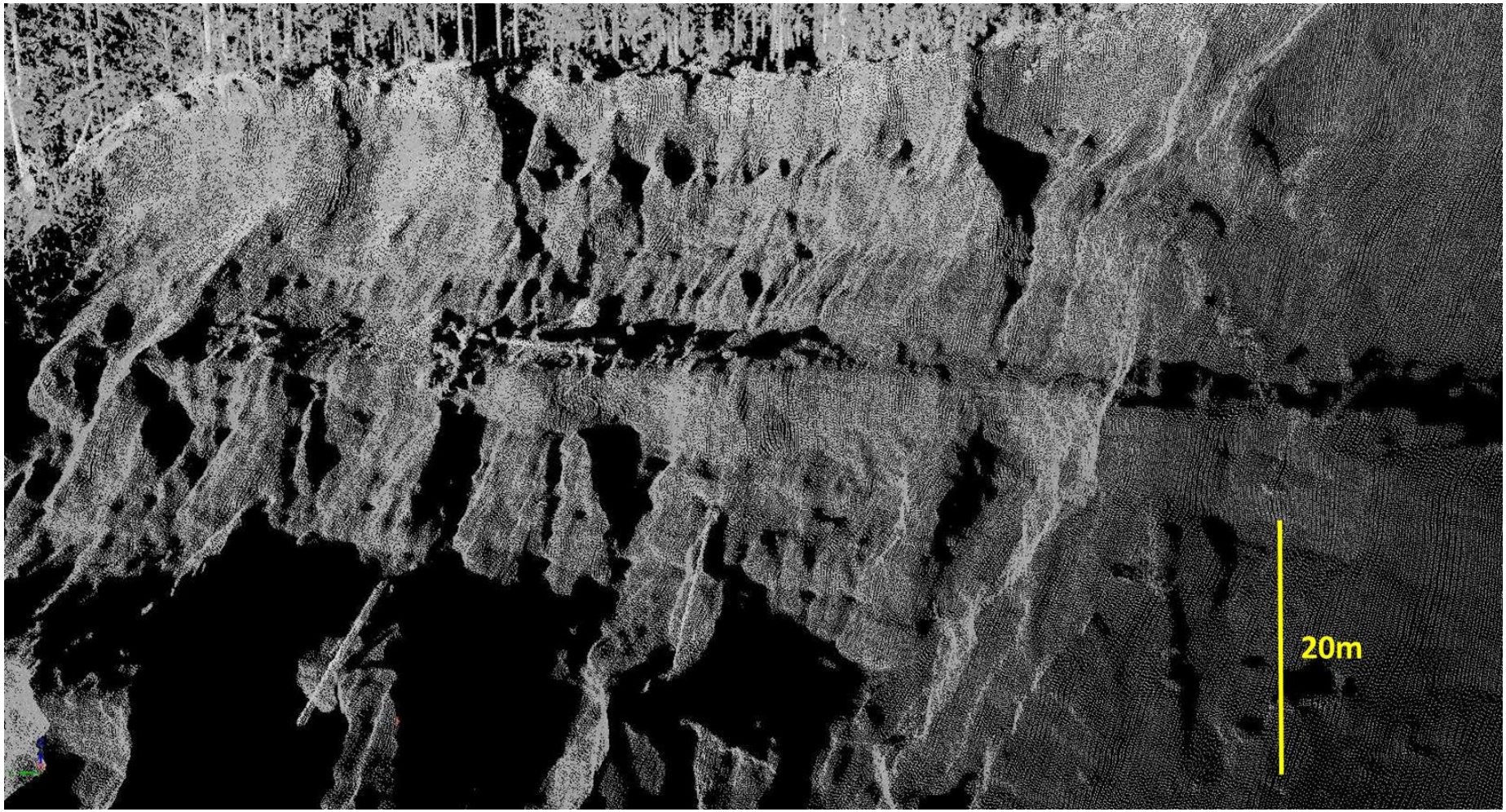

Figure 22 – Close up of 3D point cloud near the northern headwall (Figure 2). Note the visible horizontal stratigraphy running from left to right. If scanned at a higher resolution than that of the current (7-8cm), geologic mapping may be possible from kilometers away. Image is facing northwest. See Figure 19 for location.

Appendix A

Sample	GBLC - 1E						
Sieve Number	**Diameter (mm)**	**Wt. of sieve (g) (empty)**	**Wt. of Sieve w/ Materials**	**Wt. Retained (g)**	**% Retained**	**Wt. % Sum**	**% Passing**
5/8in	16	548.3	578.3	30	5.10	5.10	94.90
4	4.75	751.7	961.7	210	35.67	40.76	59.24
10	2	658.6	781	122.4	20.79	61.55	38.45
20	0.84	457.3	595.3	138	23.44	84.99	15.01
40	0.425	388.3	448.1	59.8	10.16	95.14	4.86
60	0.25	391.9	409.4	17.5	2.97	98.11	1.89
100	0.15	319.6	324.6	5	0.85	98.96	1.04
200	0.075	311.1	313.9	2.8	0.48	99.44	0.56
pan	0.01	373.5	376.8	3.3	0.56	100.00	0.00
Totals		4200.3	4789.1	588.8	100.00		

Sample	GBLC - 2G (gravel)						
Sieve Number	**Diameter (mm)**	**Wt. of sieve (g) (empty)**	**Wt. of Sieve w/ Materials**	**Wt. Retained (g)**	**% Retained**	**Wt. % Sum**	**% Passing**
5/8in	16	548.4	658.5	110.1	23.16	23.16	76.84
4	4.75	751.7	863	111.3	23.42	46.58	53.42
10	2	658.4	699.9	41.5	8.73	55.31	44.69
20	0.84	456.9	494.2	37.3	7.85	63.16	36.84
40	0.425	388.2	429.7	41.5	8.73	71.89	28.11
60	0.25	391.9	447	55.1	11.59	83.48	16.52
100	0.15	319.6	361.9	42.3	8.90	92.38	7.62
200	0.075	311.1	333.9	22.8	4.80	97.18	2.82
pan	0.01	373.5	386.9	13.4	2.82	100.00	0.00
Totals		4199.7	4675	475.3	100.00		

Sample	GBLC - 2G (Sand)						
Sieve Number	**Diameter (mm)**	**Wt. of sieve (g) (empty)**	**Wt. of Sieve w/ Materials**	**Wt. Retained (g)**	**% Retained**	**Wt. % Sum**	**% Passing**
4	4.75	751.7	765.4	13.7	7.00	7.00	93.00
10	2	658.4	681.7	23.3	11.91	18.92	81.08
20	0.84	456.9	494.3	37.4	19.12	38.04	61.96
40	0.425	388.2	422.2	34	17.38	55.42	44.58
60	0.25	391.9	433.3	41.4	21.17	76.58	23.42
100	0.15	319.3	345.5	26.2	13.39	89.98	10.02
200	0.075	311.2	323.7	12.5	6.39	96.37	3.63
pan	0.01	373.4	380.5	7.1	3.63	100.00	0.00
Totals		3651	3846.6	195.6	100.00		

Sample	GBLC-2J						
Sieve Number	**Diameter (mm)**	**Wt. of sieve (g) (empty)**	**Wt. of Sieve w/ Materials**	**Wt. Retained (g)**	**% Retained**	**Wt. % Sum**	**% Passing**
10	2	658.4	662.5	4.1	2.84	2.84	97.16
20	0.84	456.9	479.6	22.7	15.71	18.55	81.45
40	0.425	388.2	413.6	25.4	17.58	36.12	63.88
60	0.25	391.9	406.2	14.3	9.90	46.02	53.98
100	0.15	319.3	335.3	16	11.07	57.09	42.91
200	0.075	311.1	352.9	41.8	28.93	86.02	13.98
pan	0.01	373.5	393.7	20.2	13.98	100.00	0.00
Totals		2899.3	3043.8	144.5	100.00		

Appendix B

Location: Gold Basin Landslide Complex, approximately 1.5km north/northwest of Gold Basin Campground, Verlot, WA.

- Right bank/north bank of South Fork Stillaguamish River
- Scanning performed from left bank/south bank of South Fork Stillaguamish River @ Gold Basin Campground
- See Figures 1 and 2 from report

Scan Locations:

- Scan Position 1: 48.075970N, -121.73175W
- Scan Position 2: 48.0752851N, -121.7319W

File Names:

- Epoch #1: GBLC_Epoch1_20150719
- Epoch #2: GBLC_Epoch2_20150919
- Epoch #3: GBLC_Epoch3_20150110

Scan Resolutions:

- Epoch #1: 15cm respectively
- Epoch #2: 7-8cm respectively
- Epoch #3: 7-8cm respectively

Weather Conditions:

- Epoch #1:
    - Day 1: 90°F, Sunny
      Day 2: 75°F, Sunny
- Epoch #2:
    - Day 1: 60°F, Overcast/rain/fog
    - Day 2: 53°F, Foggy
- Epoch #3:
    - Day 1: 35°, Sunny, snow present on hillsides and at campground

File Name and Location:

File Name: GoldBasinLandslideData

Location 1: UWESSSTF_1 External Hardrive (TLS External Hardrive)
Part# 4064-705107-000

Location 2: “Brook” Computer in QRC Computer Lab
D:/GoldBasinLandslideData